5-2019

Full Scale 13-Story Building Implosion and Collapse: Effects on Adjacent Structures

Kanchan Devkota
University of Nebraska-Lincoln, kdevkota2@unl.edu

FULL SCALE 13-STORY BUILDING IMPLOSION AND COLLAPSE: EFFECTS ON ADJACENT STRUCTURES

by

Kanchan Devkota

A THESIS

Presented to the Faculty of

The Graduate College at the University of Nebraska

In Partial Fulfillment of Requirements

For the Degree of Master of Science

Major: Civil Engineering

Under the Supervision of

Professor Christine E. Wittich & Professor Richard L. Wood

Lincoln, Nebraska

May, 2019

FULL SCALE 13-STORY BUILDING IMPLOSION AND COLLAPSE: EFFECTS ON ADJACENT STRUCTURES

Kanchan Devkota, M.S.

University of Nebraska, 2019

Advisor: Christine E. Wittich and Richard L. Wood

Two dormitory halls at the University of Nebraska-Lincoln known as Cather and Pound halls were demolished via controlled implosion on December 22, 2017. Cather and Pound halls were two thirteen-story reinforced concrete structures. The demolition of these two structures included the implosion of controlled charges at selected columns on alternating floors which initiated the progressive collapse of these structures. Three nearby structures in the vicinity of Cather and Pound halls were instrumented with high sensitivity uniaxial piezoelectric accelerometers to record the response of the adjacent structures during the event of the implosion and the progressive collapse. While these two thirteen-story reinforced concrete structures were also instrumented with sacrificial accelerometers to record the real-time response of the structures during implosion and progressive collapse, the focus of this thesis is the responses observed at the adjacent structures during the demolition sequence. The primary objective is to understand how a group of nearby structures response and interact during the implosion and progressive collapse of multistory buildings. To this end, ground motion parameters at three free field positions nearby these adjacent structures have been quantified to observe the variation of free field ground motions during the demolition event. Likewise, the acceleration

response data obtained from adjacent structures and free field positions have been analyzed in the time and frequency domains. The analysis of response data has also been presented separately in terms of the blast and collapse sequence to differentiate and understand the response of adjacent structures during the blast and progressive collapse of the two 13-story reinforced concrete structures. An input-output study of the responses observed within three adjacent structures with respect to the ground motion recorded at free field positions indicated that secondary effects, such as the air wave generated by the blast, contributed to the structural response. Two of the adjacent structures are numerically modeled with a lumped mass approach in LS-DYNA, and the responses of these numerical models are compared to the experimental recordings. The numerical study further emphasized the significance of the air wave.

AUTHOR'S ACKNOWLEDGEMENTS

I would like to express my utmost gratitude to **Dr. Christine E. Wittich**, my advisor and thesis committee chair, for providing me an opportunity to perform research under her supervision. It has been an honor to be a part of her research group. I appreciate her for helping me to challenge myself and push the limits of my creativity and understanding in Structural Engineering. I appreciate her support, guidance and her contributions of time, ideas and funding to make my master's degree successful.

I would also like to express my utmost gratitude to **Dr. Richard L. Wood**, my co-advisor and thesis committee chair, for providing me an opportunity to begin my research at the University of Nebraska-Lincoln under his supervision. It has been my honor to be a part of his research team and receive his continuous guidance, and feedback in my research and throughout my master's studies.

I would also like to express my utmost gratitude to **Dr. Chung R. Song**, my thesis committee member, for giving his valuable time to review my work.

I would also like to gratefully acknowledge **Yijun Liao** and **Garrett P. Martindale** for their assistance in instrumentation of the adjacent structures. I would also like to gratefully acknowledge **Mr. Larry Shippen** of University of Nebraska-Lincoln University Housing and Facilities Maintenance & Operations for providing access to the adjacent structures. I would also like to gratefully acknowledge **Dr. Daniel G. Linzell** at the University of Nebraska-Lincoln and the Voelte-Keegan Professorship for his financial support and collaboration in the Cather-Pound Demolition project. I would also like to

gratefully acknowledge **Dr. Babak Moaveni** of Tufts University for providing supplemental instrumentation used in this study.

The numerical simulations conducted for this thesis were completed utilizing the Holland Computing Center of the University of Nebraska, which receives support from the Nebraska Research Initiative. I would like to express my utmost thanks to Holland Computing Center and the Nebraska Research Initiative.

The information presented in Chapter 5 of this thesis was largely taken from the conference paper: Devkota, K., Wittich, C.E., and Wood, R.L. (2019). "Full Scale 13-Story Building Implosion and Collapse: Effects on Adjacent Structures." *Proc., Structures Congress*, ASCE, Orlando, FL.

Chapters 5 and 6, in part, is currently being prepared for submission to the Journal of Performance of Constructed Facilities: Devkota, K., Wittich, C.E., and Wood, R.L. (20XX). "Effect of Ground Shaking and Air Wave on Adjacent Structures due to Building Implosion and Collapse."

Lastly, I would extend my utmost gratitude to my family for their continuous support, love, and encouragement throughout my study and my research. This accomplishment would not have been possible without them. Thank you.

Opinions, findings, and conclusions are those of the author and do not reflect those of any of the research supports and collaborators.

Kanchan Devkota

TABLE OF CONTENTS

LIST OF FIGURES

LIST OF TABLES

CHAPTER 1 – INTRODUCTION

1.1 Overview

Cather and Pound halls were two 13-story reinforced concrete residence buildings at the University of Nebraska-Lincoln that were demolished via a controlled implosion on December 22, 2017. Three adjacent structures to Cather and Pound halls were instrumented before, during, and after the implosion to study the response of the adjacent structures to blast and collapse loads as well as to examine any potential changes resulting from the ground motion due to the blast and collapse loads. Likewise, free field positions near these three adjacent structures were also instrumented to study the ground motions induced during the implosion and progressive collapse of the two buildings. While Cather and Pound halls were instrumented with sacrificial accelerometers to study the distribution of blast loads and progressive collapse, this thesis focuses on the response obtained from the three adjacent structures and their nearby free field positions. The response obtained from these three adjacent structures and their nearby free field positions have been analyzed in the time and frequency domains. The results obtained from time domain and frequency domain analysis of the captured response have been compared in terms of the blast and collapse sequence of the demolition of Cather and Pound halls. The comparative study of the acquired response in terms of blast and collapse sequence helps to understand as well as differentiate the effects of blast and collapse-induced ground motions on the structural response of adjacent structures. Likewise, the frequency domain analysis of the obtained structural response during the blast and collapse has also been presented with an input-output study to understand any

possible effects of secondary sources apart from ground motions on the observed structural response. In addition to the analysis of the experimental data, two of the adjacent structures are numerically modeled in a lumped mass approach assuming a fixed base. The models are subjected to ground motions obtained from free field positions. The numerical analyses of the two adjacent structures focuses on the significance of the contribution of the airblast wave on the observed structural response.

1.2 Motivation

The primary purpose of this study is to understand how a group of nearby structures respond and interact during the implosion and progressive collapse of multistory structures. Moving forward, results of this study could be used to guide the future design of more robust and resilience structures. However, there have not been many experimental studies where two or more full-scale buildings have been instrumented to observe the response of multiple structures to ground motions. This experimental study is a unique endeavor where three full-scale structures have been instrumented to observe their response to two different types of ground motions: blast and collapse-induced ground motions. This experimental study provides key insights over how different structures respond to these two types of ground motions which vary in terms of both amplitude and the frequency content. Another important aspect of this experimental study is the airblast wave associated with the implosion of the multistory structures. The observed response of the adjacent structures during the blast sequence of the implosion helps to clarify the possible interference of the airblast wave on the structural response. The response of the adjacent structures to ground motions is

influenced by a wide array of parameters like characteristics of ground motions, system properties of the structure, and the properties of soil domain beneath the structure. The numerical analyses of the adjacent structures based on the experimentally obtained ground motions from this study can help to improve the understanding of the dynamic response of complex real-world structures, including the combined response to ground excitation and airblast as well as the impact of soil-structure interaction.

1.3 Scopes and Objectives

The thesis consists of eight chapters.

Chapter 2 includes the literature review on soil-structure interaction (SSI), structure-soil-structure interaction (SSSI), response of structures to blast-induced ground motions and response of structures to airblast wave. The literature review forms a basis for the discussions presented in Chapter 4, Chapter 5, Chapter 6 and Chapter 7.

Chapter 3 summarizes the details of the adjacent structures, experimental setup, the location of sensors, specifications of the data acquisition used in acquiring the response data presented in this thesis.

Chapter 4 presents the system identification techniques used in the system identification of two of the adjacent structures which are primary subjects of discussion in Chapter 6 and Chapter 7. The obtained system properties of the two adjacent structures have been used in Chapter 6 and Chapter 7 to interpret the observed responses in the frequency domain. Likewise, these system properties of the two buildings have also been used in the calibration of the numerical models of these buildings in Chapter 7.

Chapter 5 presents the response data obtained from the three adjacent structures and their respective free field positions using time domain and frequency domain analysis. A primary objective of this chapter is to compare and observe the variation of responses within the three adjacent structures and free field positions near these adjacent structures.

Chapter 6 presents an input-output study of the observed response within the adjacent structures with respect to observed response at respective free field positions of these adjacent structures. The goal of this chapter is differentiating and understanding the response of the adjacent structures to the blast and collapse-induced ground motions. Likewise, the purpose of this chapter is also to understand and interpret the high mode response of the structures observed during the blast sequence.

Chapter 7 includes the numerical modeling of two adjacent structures using the two -degree of freedom (2DOF) lumped mass model approach. The purpose of this chapter is to study the numerical response of the adjacent structures when subjected to the experimentally obtained ground motions from the free field positions.

Chapter 8 summarizes the key observations and conclusions made from the study presented in this thesis.

CHAPTER 2 – LITERATURE REVIEW

2.1 An overview

The study focuses on the response of the nearby structures during the controlled implosion and collapse of two 13-story reinforced concrete structures. While both implosion and collapse can induce ground motions, a part of the energy released during the implosion can also give rise to the airblast wave. The thesis touches upon some key areas of research associated with the response of nearby structures to ground motions as well as the response of structures to the airblast wave. These key areas of research include:

- Soil-Structure Interaction (SSI)
- Structure-Soil-Structure Interaction (SSSI)
- Response of structure to blast and progressive collapse induced ground motions
- Response of structure to the airblast wave.

A brief discussion of each of these areas of research has been provided in the subsequent sections included in this chapter.

2.2 Soil-Structure Interaction (SSI)

The response of a structure subjected to ground motion, such as an earthquake, cannot be defined by the parameters related to the structure alone. The degree by which the structural response is influenced by ground motions depends upon a wide array of

factors like the flexibility of the structure, its foundation, and the soil, as well as the ground motion that is introduced to the structure through the soil domain. This makes soil-structure interaction (SSI) a complicated phenomenon with a higher number of degrees of freedom than for a structure alone. SSI is usually explained under two aspects: kinematic interaction and inertial interaction. Kinematic interaction refers to the modification of the input ground motion due to the presence of a stiff foundation in the soil; and, inertial interaction refers to the modification of structural response due to the presence of a flexible soil domain on which the structure is founded. Traditionally, structures are often designed with an assumption that they are founded rigidly on a stiff soil. However, the response of a structure founded on a stiff soil to a ground motion can be noticeably different than the response on a relatively flexible soil domain. The structures with foundation on flexible soil have longer natural periods of vibration when compared to structures with foundation on relatively stiff soil. This is due to the inertial interaction between the soil and structure where a substantial amount of vibrational energy of the SSI system is dissipated due to the hysteretic material damping of the soil domain and the radiation of incident ground motion waves from the structure-soil interface. The effect of soil-structure interaction can be more pronounced in very rigid structures like the structures containing nuclear structures. Although the rigid structure may lie on relatively firm soil, the relative stiffness between the structure and its foundation can play a significant role in the modification of structural response (Jennings and Bielak 1973). As nuclear powerplants are heavy and stiff, they create a more suitable scenario for the occurrence of SSI. Most of the previous research work in SSI in past

decades have been stimulated by a greater safety concern towards the vulnerability of nuclear power plants towards SSI.

However, recent research developments have begun focusing on the effects of SSI on typical building structures as well. Dutta et al. (2004) did a numerical study to examine the effects of SSI on buildings with isolated and grid foundations when subjected to seismic excitations. The study showed an increase in base shear due to SSI in low-rise buildings and decrease in base-shear in mid to high-rise buildings due to SSI. Likewise, the study indicated that pulse-like near fault ground motions with short period pulses (period less than 1s) resulted in an increase in seismic demand due to soil-structure interaction. The flexibility of the soil domain can change the effective natural period of any buildings where the change in natural period largely affects the seismic response of the building. The effect of the lengthening of the natural period due to SSI in low-rise structures can make these structures vulnerable to seismic excitation if SSI is not taken into account in the seismic design (Bhattacharya et al. 2004). Contrary to the traditional design assumption, the ductility demand of a structure does not always decrease with decrease in the natural period of the structure due to SSI (Mylonakis and Gazetas 2000). This indicates that the study of effects of SSI on the response of buildings is pivotal to ensure safety of the buildings during seismic events. The numerical studies and experimental studies done regarding SSI are detailed in Section 2.2.1 and Section 2.2.2.

2.2.1 Numerical Methods in SSI: An Overview

In the study of dynamic building-soil interaction by Jennings and Bielak (1973), the authors presented a method to calculate the earthquake response of multistory

structures where the soil domain is modeled using a linear elastic half-space and the n-story structure foundation system is modeled using n+2 single degree of freedom, viscously damped, linear oscillators founded on a rigid ground. The study showed that the effect of soil-structure interaction may not always decrease the maximum response of a structure. The soil-structure interaction could result in an increase in the response of structure when there is an increase in the effective damping of the soil-structure system. Gazetas (1991) derived a set of algebraic formulas to calculate the dynamic impedance functions for different shapes of rigid foundations in a homogenous half-space, for significant translational and rotational modes of vibration and using a realistic range of Poisson's ratio. The dynamic impedance functions represent the damping and stiffness characteristics of the foundation-soil interaction system (Kramer and Stewart 2004).

With the development of powerful computing tools, finite element methods and boundary elements methods were introduced in SSI, and this allowed the calculation of impedance functions for complex foundation shapes and different types of soil-structure configurations. The impedance function is one of the substructures used within the Substructuring method. The substructuring method is a sophisticated method to model SSI phenomenon where the soil-foundation-structure system is divided into different substructures and the response from each substructure is superimposed to obtain the final response of the soil-foundation-structure system. Although the Substructuring Method is computationally efficient, it can be only used in the linear analysis of SSI phenomenon. The direct Method is another prominent approach towards SSI analyses that allows a more realistic simulation of non-linear aspects of SSI. Finite Element programs like LS-DYNA (LSTC 2019) can be used to model SSI using the Direct Method, where the entire

soil-structure system is modeled at once in contrast to the superposition method employed in Substructuring method. Details on the Substructuring Method and Direct Method as well as discussion of recent research efforts in these domains are discussed in Section 2.2.1.1 and Section 2.2.1.2 respectively.

2.2.1.1 Substructuring Method: SSI

The response of a structure to ground motions is influenced by the interaction between the structure, foundation and the soil domain beneath the foundation (Kramer and Stewart 2004). In the substructuring method, the SSI system is broken down in different substructures where the response of each substructure is calculated independently and then superimposed to find the total response of an SSI system. Kramer and Stewart (2004) listed three steps for SSI analysis using the substructuring method as follows:

- *Evaluation of foundation input motion* (FIM): This step includes the evaluation of the input motion at the base of the foundation if the structure and foundation were massless. Once FIM is determined, a transfer function is calculated that represents the variation of FIM from free field motion.
- *Determination of the impedance function*: Impendence function represents the stiffness and damping characteristics of the foundation-soil interaction system. The impedance function is determined based on the properties of soil stratum and the stiffness and geometry of the foundation.

- *Dynamic analysis*: This includes the dynamic analysis of the structure excited with FIM at its base where the base of the structure is represented by the impedance function.

  These three steps have been interpreted in Figure 2.1:

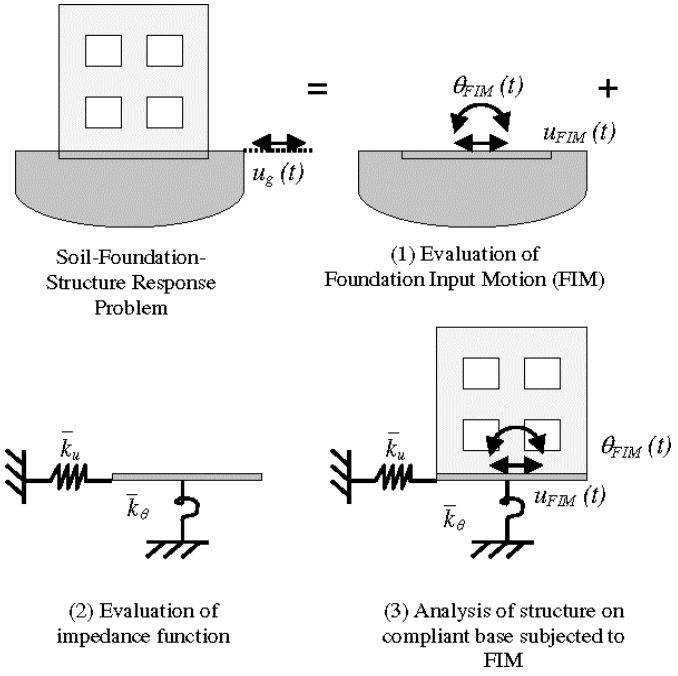

Figure 2.1: Substructuring method in SSI. (Kramer and Stewart 2004)

2.2.1.2 Direct Method: SSI

In the direct method of SSI analyses, the entire SSI system is analyzed in a single step. While the detail steps for the direct method of SSI analyses can be found in Bolisetti and Whittaker (2015), only key numerical parameters and challenges with regard to the direct method of SSI analyses has been discussed here. In this method, the structure is modeled over an infinite soil domain where ground motion is applied as force input at the bottom of the soil when modeled with a viscoelastic bedrock assumption and as an

acceleration input when modeled with a rigid bedrock assumption (Bolisetti and Whittaker 2015). Although the modeling of infinite soil domain is a challenge, this can be done defining a large enough finite soil domain such that the waves radiated from the structure do not reflect from the boundaries of the soil domain. In addition to that, the boundaries of the finite soil domain should account for the stress equilibrium conditions of the remaining soil domain that has not been included to make the soil domain finite from infinite. Figure 2.2 shows the finite element model of an SSI system using the direct method.

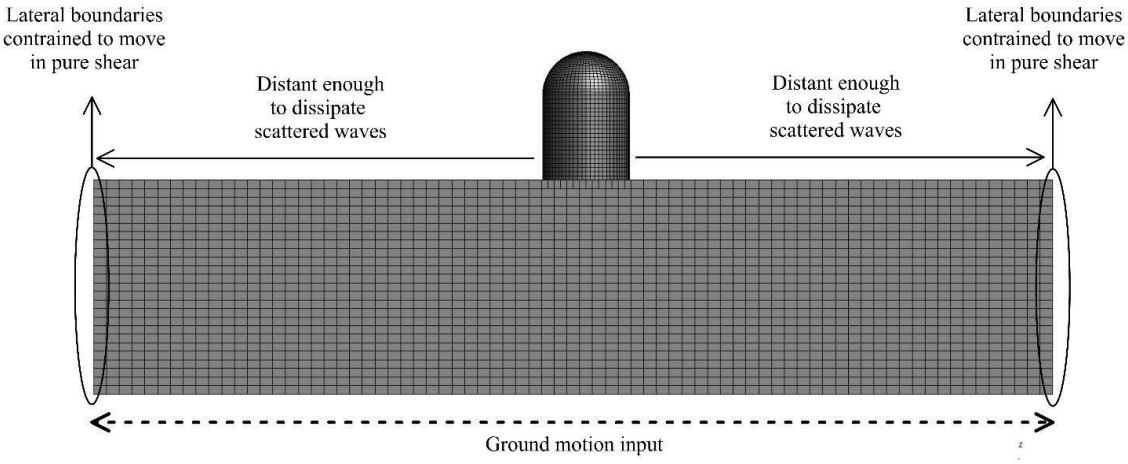

Figure 2.2: Direct method in SSI (Bolisetti and Whittaker 2015)

2.2.2 Experimental Studies in SSI: An overview

Trifunac et al. (2000) presented analytical procedures to evaluate SSI effects in a structure with an embedded foundation and used system identification results to validate these analytical procedures through empirical findings. A total of 77 strong motion recordings for 57 sites in California and Taiwan were used in the system identification

analyses in this study where fixed- and flexible-base modal vibration parameters of the SSI system were calculated. The study showed that inertial SSI interaction was evident in some structures where the ratio of flexible-base modal period of the structure to its fixed-base modal period was approximately 4. de Barros and Luco (1995) used forced vibration tests performed on on a cylindrical reinforced concrete shell structure with a circular slab foundation to calculate the foundation impedance functions and compare the observed structural response with the theoretical response calculated based on identified soil properties and structure models. The theoretical response derived from the experimentally-based impedance functions matched reliably with the structural response. The study concluded that the impedance functions vary depending upon the soil properties and the contact conditions along the base of the foundation.

Pitilakis et al. (2004) attempted to validate the numerical response of an SSI system using a centrifuge experiment involving a scaled single-degree-of-freedom structural model. The experiment was carried out under a high gravitational environment of 50g to simulate the response of a full-scale structure and soil domain. This study presented comparative results that had good agreement between the experimental and numerical response particularly in the time domain. However, some differences were observed in the frequency domain which was attributed to the difference between the predominant frequencies of the model and input motion and to nonlinear response of the soil domain.

Pitilakis et al. (2008) used the numerical code MISS3D (Clouteau and Aubry 1992, 2003) to numerically simulate the SSI phenomenon that was studied with shake table test in the BLADE laboratory at the University of Bristol. The shake table test

included a model of foundation-structure system embedded in dry bed sand subjected to strong ground motion. The numerical simulation that was carried out using the substructuring approach with a linear viscoelastic domain reliably estimated the recorded experimental response in the soil deposit although nonlinear soil behavior is expected during strong ground shaking. Likewise, the numerical response and experimental study both showed a decrease in the acceleration forces at the top of the structure. The decrease in the acceleration forces at the top of the structure has been attributed to the primary effects of SSI: decrease in the stiffness of foundation-structure system and the increase in the damping.

2.3 Structure-Soil-Structure Interaction (SSSI)

SSSI is an extension of SSI where two or more adjacent structures founded within the same soil domain interact with each other when the soil domain is subjected to dynamic motion. When a structure is subjected to ground motion, some part of the vibrational energy of the structure is radiated into the soil domain through a soil-foundation interface which may lead to the dynamic interaction between adjacent structures that are built within same soil domain. In cases where several structures are clustered together, the dynamic response of one structure may not be independent of the adjacent structures since there is a greater possibility of interference of the structural responses through the soil. Although there has been notable progress in the study of SSI in recent decades, advances in the research of SSSI is quite limited. While SSI is extensively considered in the design of nuclear power plants, SSSI is not considered. Although it cannot be confirmed whether SSSI is conservative or non-conservative in

terms of seismic demands on structure, SSSI has gained much more attention within the research community in recent decades.

2.3.1 Numerical Methods in SSSI: An Overview

Luco and Contesse (1973) presented a numerical study on SSI problem using two parallel infinite shear walls founded on rigid foundations of semi-circular cross section and subjected to vertically incident plane SH wave with harmonic time-dependence. The paper presented parametric studies to conclude that the interaction effects are prominent when a small shear wall is at close proximity with a larger shear wall. Wong and Trifunac (1975) followed the work of Luco and Contesse (1973) to study the significance of angle of incidence of incident SH waves along with the effect of the relative size and natural frequencies of neighboring structures, and the effect of relative distance between foundation on the interaction between two or more shear walls. The study showed that scattering, diffraction and interference of waves from and around several foundations with incident SH waves can alter the free field motion and the presence of other buildings can produce significant change on the single soil-structure interaction problem. With the rise in powerful computing resources, FEM has been used extensively in the numerical modeling of SSI as well as SSSI systems. Matthees and Magiera (1982) performed a sensitivity study using finite element method with computer code FLUSH where they studied the interaction between the adjacent structures of the nuclear power plant due to horizontal seismic excitation. The results obtained from the study showed that specific frequency behavior of the structure can have a significant influence on SSSI especially in case of small depth of soil. Lin et al. (1987) performed an analytical parametric study on

the interaction between adjacent foundations based on the effects of distance, the direction of alignment, embedment depth and structural inertia on SSSI. The inertial interaction induced due to the supported structure on each foundation increased with a decrease in distance between the adjacent foundations as well as the increase in the embedment depth of the foundations. A decrease in characteristic frequency of the foundation-structure system was more pronounced when two square foundations were aligned side by side than when aligned diagonally.

Apart from the Finite Element Method (FEM), Boundary Element Method (BEM) has also been practiced actively to model SSSI problems. One notable advantage of BEM over FEM is that it only requires the discretization of the surface of the domain while FEM requires the discretization of the surface as well as the interior of the domain. BEM automatically considers the radiation condition at infinity Beskos (1993). This advantage is particularly useful while modeling a three-dimensional infinite domain in SSI and SSSI problems which might result in inaccuracy with FEM. Karabalis and Mohammadi (1998) built upon previous works and studied the dynamic response of single and multiple foundations on a layered viscoelastic soil domain using 3-D frequency domain BEM. The study concluded that foundation-soil-foundation interaction is more prominent when the soil domain consists of thin soil layers near the surface.

FEM has also been coupled with BEM to use the advantages of both numerical approaches in SSSI studies. Wang and Schmid (1992) used coupled FEM-BEM to study the dynamic interaction between three-dimensional structures through the underlying soil. In the study, the structure and foundation were discretized using FEM, and the soil domain was discretized using BEM. The paper demonstrated the effect of distance

between structures, the influence of the natural frequency of the soil domain as well as the natural frequency of structures and the location of excitation load on SSSI. Lehmann and Antes (2001) studied the suitability of coupled BEM-FEM approach to model SSSI problems where the soil was approximated by using three-dimensional Symmetric Galerkin Boundary Element Method (SGBEM), and multi-story buildings were modeled using FEM. Likewise, Padron et al. (2009) presented a study on the dynamic interaction between pile supported structures under incident S wave and Rayleigh waves using three-dimensional viscoelastic BEM-FEM formulation. The paper concluded that SSSI effects can be sensitive for a group of structures with similar dynamic properties, especially at the fundamental frequency of the overall system. Similarly, the highest amplifications were noted around the central constructions when the incident waves produced motion along the direction of alignment of the structures.

2.3.2 Experimental Studies in SSSI: An Overview

There have been a minimal number of experimental campaigns to study SSSI when compared to numerical studies done in SSSI or SSI. Kobori et al. (1977) carried out vibrational field tests for two identical foundations under the harmonic excitation by a vibration generator where responses were recorded using velocity type seismometers. The theoretical dynamic vibrational characteristics were obtained using ground compliance matrix of the foundation on a visco-elastic half-space and then compared with the experimental evidence. The study pointed out that cross-interaction effects are significant over the wide frequency range when the distance between the foundations decreases.

Mizuno (1980) experimented for SSSI to study the effects of radiation waves from a structural system and energy absorption by natural mode excitation of a structural system. A model reinforced mat foundation and a model reinforced mat foundation with a superstructure were constructed nearby an existing full-scale three-story steel frame building to study SSSI based on forced vibration tests, microtremor measurements and earthquake observations. The microtremor measurements of the experimental study were compared with foundation displacements and relative displacements of the superstructures obtained from the analytical study. Both experimental results and analytical results confirmed the SSSI between structures in earthquakes. The paper concluded that radiation of waves from other structures can have notable effects on the response of structures. Likewise, the study also highlighted that the energy absorption capacity of the structure from the ground, when excited in its own mode, can have significant SSSI effects.

Celebi (1993a, 1993b) studied SSSI between two adjacent seven-story buildings in Norwalk, California due to Whittier-Narrows, Calif. Earthquake of 1987. This study is a rare experiment in the field of SSSI research that was performed with full-scale buildings during a real earthquake. Acceleration responses during the earthquake were obtained from the roof and basement of the two adjacent structures and three free field positions using strong motion accelerographs. Spectral analysis of these acceleration responses was done where cross-spectra and coherence functions were computed to compare the acceleration responses obtained from the two adjacent structures and free field positions. The experimental study concluded that structure-soil-structure interaction was evident between the two adjacent structures as a result of the two adjacent structures

resonating into the Rayleigh frequencies of the ground. The author indicated the occurrence of structure-soil-structure interaction at specific frequencies in the cross spectra and high coherence of responses of various free-field locations and locations within two adjacent structures.

Bolisetti and Whittaker (2015) presented a detail report on a comparative study between the numerical modeling of SSSI and experimental results obtained from the experimental program of the NEES City Block project. The City block project included six centrifuge tests targeted to examine SSI and SSSI among which results from Test 3 and Test 4 have been used by Bollisetti and Whittaker (2015) to compare with the results obtained from numerical platforms: SASSI and LS DYNA used to model SSSI and SSI in the study. Test 1 used a one-story building model with spread footings and a three-story building model with a basement to examine the SSI effects. Likewise, in Test 2 the same two models were kept adjacent to each other and parallel to the shaking motion to study SSSI effects between them. Test 3 used a heavy and stiff structure placed adjacent to light and flexible structure to study SSI and SSSI effects. Likewise, Test 4 includes five different structures on dry, dense sand representing a complete city block. Ganuza (2006) and Chen et al. (2010) include the details of the design and development of the prototype buildings and the model structures used in the City Block project. The design procedures for the models used in this centrifuge experiment can be found in Bolisetti (2010). No distinct dynamic interaction between the structures could be observed in the numerical studies and experimental responses obtained from Test 3 and Test 4 (Bolisetti and Whittaker 2015). Bolisetti and Whittaker (2015) also pointed out that restraining of footing from adjacent basements might result in local SSI effects that could produce

significant changes in global structural response. Further, the paper also concluded that the accurate prediction of structural response to intense ground motions is sensitive to the numerical modeling of foundation nonlinearity mechanisms like footing sliding and gapping.

2.4 Response of structures to blast-induced ground motions

The blast can induce ground motions resulting in the vibration of nearby structures. The ground motion characteristics for seismic waves generated by earthquakes can vary from the ground motion characteristics for blast-induced seismic waves. Primarily, the blast-induced seismic waves have a shallower hypocenter when compared with earthquake-generated seismic waves. Hao et al. (2001) computed coherency and cross-correlations between the blast-induced ground motions along same directions recorded on locations on ground surface separated by a distance of 25 m. The blast-induced ground motions along the same directions indicated a weak correlation contrary to seismic ground motions which show high correlation (Abrahamson 1985) along the same directions. The acceleration time histories recorded at these two locations that were 25 m apart also indicated quick attenuation of the amplitude of the blast-induced ground motions. The higher spatial variation and quick attenuation of blast-induced ground motions have been attributed to its high-frequency content where the ground motions are greatly influenced by the heterogenous propagation media.

Regardless of the source of the ground motions, the response of a structure is influenced broadly by the characteristics of the ground motion. Blast-induced ground motions can possess high risks to nearby structures if the ground motion has low-

frequency content to result in resonance with the structure. However, experimental studies regarding blast-induced ground motions have shown that blast-induced ground motions tend to have very high frequencies. Nateghi (2011) has presented a study on ground motions induced by near underground and surface concrete structures during the construction of a dam. The study found that all the blasts that were observed had frequency content higher than 20 Hz such that the damage risk on surrounding structures due to resonance was minimum. The response of the structure to blast-induced ground motions could be amplified or attenuated with respect to the amplitude of input ground motions depending upon the frequency content of the ground motions and the size of the footprint of the structure. While the responses observed at the top of structures were attenuated when subjected to high-frequency excitation pulses, the responses at the top were amplified in the case of smaller residential structures when subjected low-frequency excitation pulses with a frequency closer to the natural frequency of the structure (Dowding et al. 2018).

Siskind et al. (1980) have also shown that the structural response tends to show amplification with respect to blast-induced ground motions that have a low-frequency content of 4 Hz to 10 Hz which is also a typical range of natural frequencies for residential structures. Although the frequency of blast-induced ground motions typically exceeds the natural frequencies of most non-residential building structures, i.e. 4 Hz to 10 Hz, the study showed that low-frequency ground motions due to the blast were more evident with the increase in distance from the blast site. The amplification of structural responses with typical amplification factors ranging between 1.5 to 4 was observed for blast-induced ground motions with principal frequencies between 4 Hz to 10 Hz.

However, the structural response amplification factors were less than unity for blast vibrations with principal frequencies above 40 Hz.

2.5 Response of structures to airblast

Apart from the blast-induced ground motions, airblast wave is also a secondary effect of the blast. It can be challenging to measure the effect of the airblast wave on a structure where the response is usually dominated by the response to ground motions during the blast. The shock from airblast travels through the atmosphere as a compression wave and can be related to P-wave traveling through the earth (Elseman 2000).

The effect of the airblast wave on a structure is greatly influenced by the weather conditions for propagation. Since the propagation of the airblast wave greatly varies depending upon the blast confinement and airblast character and levels, the study of the effect of airblast wave is comparatively challenging than the study of blast-induced ground motions (Siskind et al. 1980). Siskind et al. (1980) performed an experimental study where the responses of residential structures to the airblast wave generated from mining operation were studied to design blast to have a minimal effect on surrounding structures. The study included the observation of 56 different structures where low-frequency pressure transducers of 0.1 Hz to 380 Hz was used to obtain airblast time histories. The time histories included the airblast measured in terms of time-varying overpressure where overpressure was also related to the relative sound level in decibels (dB). The study has presented safe airblast levels in decibels (dB) for structure by comparing with the equivalent vibration level of the structure to ground motions. Table 2.1 shows airblast sound levels compared with the response of the structure to ground

vibration with equivalent damage risks for different types of blast and structures with different story heights. Three different approaches are presented in Table 2.1 where the first approach compares the mean values of the airblast and ground vibration plates. For example, if we consider a mine blasting and a 2-story structure, the airblast level equivalent to peak particle velocity of 0.5 in/s is 139 dB (0.1Hz), 137 dB (2Hz), 135 dB (6 Hz) and 112 dB (for airblast not exceeding 2 s duration). The second approach gives these airblast levels with a minimal probability of the most the superficial type of damage on a structure provided that the ground vibration response of the structure is accompanied by the riskiest situations which include low-frequency vibrations of structures located on soft soil.The third and final approach included in this study approach provides these airblast levels based on the maximum airblast values and mean ground responses. Likewise, the peak particle velocities (equivalent vibration) of 0.5 in/s, 0.75 in/s and 1.0 in/s presented in Table 2.1 correspond to a frequency of 10 Hz assuming a simple harmonic motion.

Faramarzi et al. (2014) presented an experimental study of the response of nearby structures to the blast-induced ground motions in conjunction with the effect of airblast on those structures. The experimental study measured peak particle velocity (PPV) using peak vector sum of the three orthogonal velocity components from 22 blast sites along with the frequencies, duration of vibrations and air over pressure levels for each of the events. The blast-induced ground motions had 49 % of blast frequencies between 1 to 4 Hz, 45 % of them were between 4 to 14 Hz, 60 % of them were between 14 and 40 Hz with no frequency over 40 Hz. Figure 2.3 shows the observed peak particle velocity with respect to the frequency at 22 sites overlaid with safe blast levels provided by United

States Bureau of Mines (USBM) (Siskind et al. 1980) in terms of PPV and frequency of ground motions. Figure 2.3 indicates that PPV exceeded safe airblast levels at some sites. With the majority of frequency of blast-induced ground motions well within the frequency range of 1-14 Hz and PPV exceeding the safe limits prescribed by USBM, some X-cracks and plaster failure were observed in a building near the blast sites that exceeded the PPV levels prescribed by USBM. The airblast data obtained from the study indicated a maximum noise level of 122 dB which is under the safe limit of 164 dB for glass breakage as per USBM. The airblast-induced noise showed indicated frequencies less than 15 Hz that could cause rattling of windows in nearby structures.

Table 2.1: Airblast sound levels for control of structure response based on ground vibration response and damage levels (Siskind et al. 1980)

Type of blasting	Structures	Equivalent vibration, in/sec	Sound levels, lb/in^2 (dB)				Assumptions
			0.1 Hz	2 Hz	6 Hz	C-slow	
Mine.....	All.....		0.0195 (137)	0.0171 (135)	0.0126 (133)	0.00133 (113)	Utilized mean values of both airblast response and ground vibration response.
	1-story.		.0164 (135)	.0144 (134)	.0109 (132)		
	2-story.		.0272 (139)	.0198 (137)	.0154 (135)	.00115 (112)	
Quarry....	All.....		.0237 (138)	.0210 (137)	.0156 (135)	.0017 (115)	
	1-story.		.0206 (137)	.0183 (136)	.0138 (134)		
	2-story.		>.018 (>136)	.026 (139)	.024 (138)	.0012 (112)	
Mine.....	All.....	>0.50	.0093 (130)	.0073 (128)	.0045 (124)	.00037 (102)	Based on 5-percent probability of strong response to airblast and weak response to ground vibration. This is the least favorable airblast case. All other predictions give higher airblast levels.
	1-story.		.0080 (129)	.0063 (127)	.0039 (123)		
	2-story.		.0153 (135)	.0107 (131)	.0080 (129)	.00065 (107)	
Quarry....	All.....		.0161 (135)	.0136 (133)	.0094 (130)	.00088 (110)	
	1-story.		.0131 (133)	.0110 (132)	.0076 (128)		
	2-story.		>.017 (>135)	.0207 (137)	>.012 (>132)	.00130 (113)	
Mine.....	All.....	>1.0	.0225 (138)	.0193 (137)	.0139 (134)	.00144 (114)	
	1-story.		.0186 (136)	.0160 (135)	.0116 (132)		
	2-story.		>.017 (>135)	>.020 (137)	>.012 (>132)	>.0015 (>114)	
Quarry....	All.....		>.025 (>139)	>.020 (137)	>.015 (>134)	>.0015 (>114)	
	1-story.		>.025 (>139)	>.020 (137)	>.015 (>134)	>.0015 (>114)	
	2-story.		>.017 (>135)	>.020 (137)	>.015 (>134)	>.0015 (>114)	
Mine.....	All.....	>0.75	.0193 (136)	.0166 (135)	.0109 (132)	.00077 (109)	Based on maximum airblast values (envelope of measured data) and mean ground vibration responses.
	1-story.		.0151 (134)	.0127 (133)	.0082 (129)	.00053 (105)	
	2-story.		>.020 (>137)	>.020 (>137)	>.020 (>137)	>.0007 (>108)	
Quarry....	All.....		~.029 (140)	~.029 (140)	~.029 (140)	>.0012 (>112)	
	1-story.		.0241 (138)	.0211 (137)	.014 (134)	.00105 (111)	
	2-story.		>.020 (>137)	>.020 (>137)	>.020 (>137)	>.0007 (>108)	

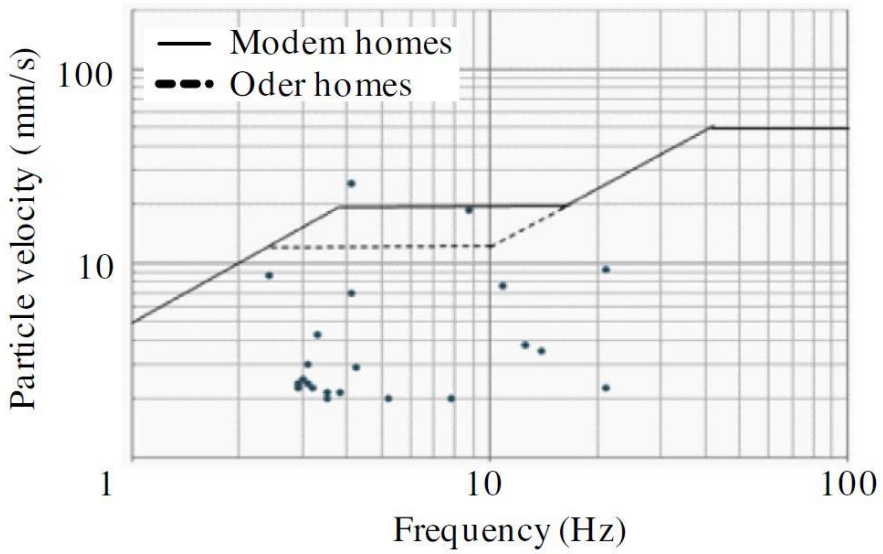

Figure 2.3: Peak particle velocity (PPV) with respect to frequency at 22 blast sites (Faramarzi et al. 2014)

2.6 Justification

The experimental study presented in this thesis includes the response of three nearby structures to ground motions induced due to the controlled implosion and progressive collapse of two 13-story reinforced concrete residential buildings: Cather and Pound Halls at the University of Nebraska-Lincoln. The study also initiates a discussion on the possible secondary effects of the airblast wave on the structural response of nearby structures during the implosion of blast charges in the two 13-story structures. Acceleration responses were recorded from the nearby free-field positions and within the nearby structures during this demolition event. Likewise, ambient responses were also obtained from the free-field positions and within the three adjacent structure both before and after the demolition event. While there has been a good amount of research related to

the progressive collapse of structures, there have not been many experimental studies that have documented the response of nearby structures to the progressive collapse of multistory structures. Similarly, most of the studies regarding the response of nearby structures to blast-induced ground motions have been based on the surface or underground explosions occurring in the mining industry. A unique combination of the effect of the progressive collapse and above-ground implosion of multistory buildings in the surrounding structures makes the experimental study included in this thesis a very rare pursuit of research.

The dataset obtained from the adjacent structures during the implosion and progressive collapse of Cather and Pound halls can provide a good insight over SSI as well as SSSI research. The structural responses observed within each of the adjacent structures and the responses observed at free field positions during the demolition can help to gain a better understanding of the effect of the soil domain on the structural response. Likewise, the experimental study includes a cluster of 3 adjacent structures. The study of responses observed in such a cluster of structures to the ground motions induced from blast and collapse would be a key step forward in understanding the response of structures in an urban environment against the individual response of the structure to ground motions.

To sum up, the study is unique since it encompasses real-time large-scale experimentation of the multi-building response to blast and progressive collapse. Further, the study is a noble approach towards the understanding of the response of nearby structures to blast, collapse and airblast simultaneously.

CHAPTER 3 – EXPERIMENTAL DESIGN

3.1 An Overview

Two 13-story reinforced concrete residence halls at the University of Nebraska-Lincoln: Cather (40.819015N, -96.696895E) and Pound (40.818161, -96.696920E) halls were demolished with controlled implosion on December 22, 2017. Sacrificial accelerometers were installed within the two 13-story structures to study the distribution of blast loads and the progressive collapse of these two structures. Likewise, three structures adjacent to Cather and Pound halls were also selected to study the response of the adjacent structures during the implosion and progressive collapse of the two 13-story structures. The three adjacent structures and free field positions near each of these adjacent structures were instrumented before, during and after the implosion and collapse of the Cather and Pound halls. The study presented in this thesis focuses on the study of the response observed at the three adjacent structures during the implosion of Cather and Pound halls. In addition to the study of the structural response of these adjacent structures during the implosion, the ambient vibration data collected from these adjacent structures prior to the implosion have been used in the system identification of the adjacent structures. This chapter includes the details of the three adjacent structures and the instrumentation setup used to obtain the response data discussed in this thesis.

3.2 Buildings and Instrumentation

Three adjacent buildings selected for the study were Neihardt Residential Center (40.818587N, -96.697306E), Willa Cather Dining Center (40.818407N, -96.696013E),

and Abel Hall (40.821945N, -96.696117E). Each of the three adjacent structures alongside with Cather and Pound halls is shown in Figure 3.1. Neihardt Residential Center will be referred as Building A, Willa Cather Dining Center will be referred as Building B and Abel Hall will be referred as Building C throughout this thesis. A total of 21 high sensitivity seismic uniaxial piezoelectric accelerometers were used to record the response of the above mentioned three adjacent structures before, during and after the implosion of Cather and Pound. The general layout of Building A, Building B, Building C and Cather and Pound halls is shown in Figure 3.1 and the layout of these buildings obtained from Google Earth is presented in Figure 3.3.

(a) (b) (c) (d)

Figure 3.1: Instrumented Buildings: (a) Cather Hall (right) and Pound Hall (left), (b) Neihardt Residential Center, (c) Willa Cather Dining Center, (d) Abel Hall.

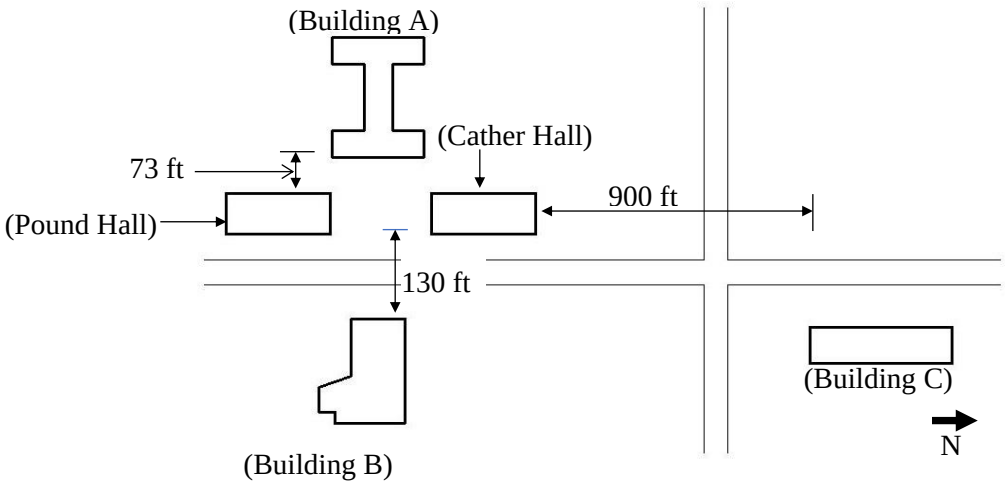

Figure 3.2: General layout of instrumented buildings

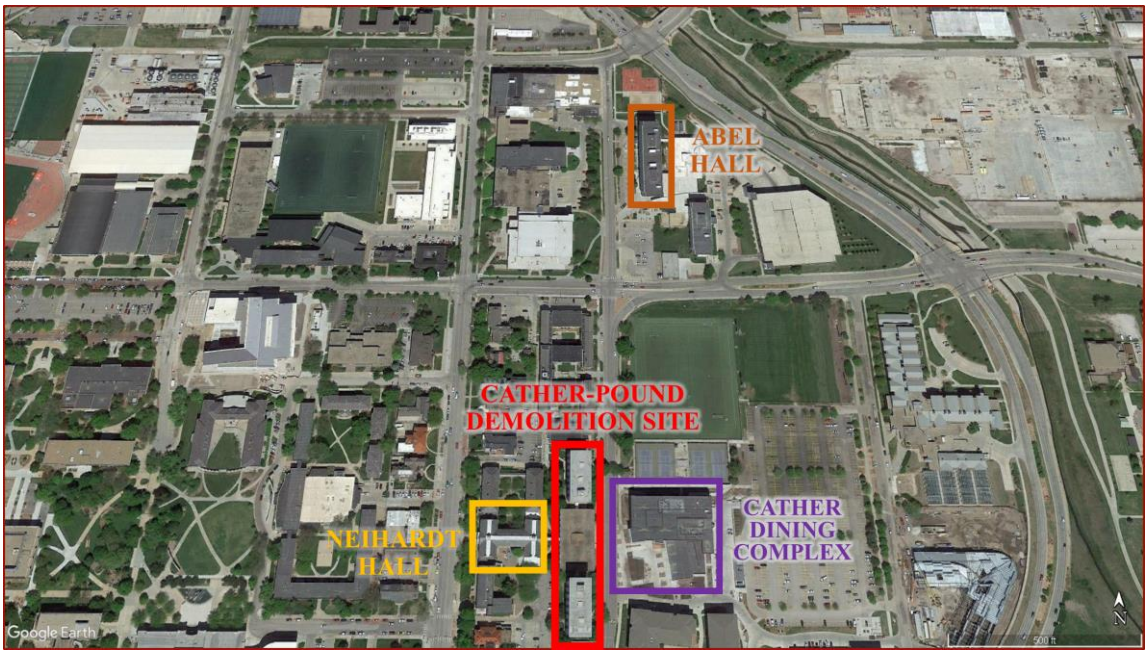

Figure 3.3: General layout of instrumented buildings (Google Earth view)

Building A is a three-story reinforced concrete frame building with unreinforced brick masonry exterior walls which was constructed in the fall of 1932- see Figure 3.1b. It is located approximately at an offset distance of 73 ft towards the west of Cather and Pound. The height of the building is 44.5 ft including the basement. Typical plan for the Building A along with the sensor setup is shown in Figure 3.4a. Two perpendicular accelerometers were installed at each of the four corners at the roof of Building A to measure the N-S and E-W acceleration as well as to observe if there is any torsional response. Figure 3.4a also shows FF. Pos. 1 where three perpendicular accelerometers were installed on the ground adjacent to east facade of Building A to record N-S, E-W and vertical motions of the ground.

Building B is a three-story steel framed building with a basement and founded on pile foundation. The building was constructed in 2017 and has a total height of 61ft from

the basement. The building is located on the east side of the Cather and Pound at an offset distance of 130 ft approximately. Two perpendicular accelerometers were installed on the third floor of Building B facing N-S and E-W direction and other two perpendicular accelerometers were installed on ground floor. A typical plan of the building along with details of sensor setup is shown in Figure 3.4b.

Building C is a thirteen-story reinforced concrete frame building with a total height of 136 ft from the basement. The building was constructed in 1963 and it is located towards the north of Cather and Pound at an offset distance of 900 ft from the northernmost point of the site. Four accelerometers were installed on the roof of Building C. The building has two elevator shafts where a pair of N-S and E-W accelerometers were installed on roof level of each elevator shaft. A typical plan for the building along with the layout of the sensors used is shown in Figure 3.4c also shows FF. Pos. 3 where a pair of two N-S and E-W accelerometers were installed on the ground floor of Building C.

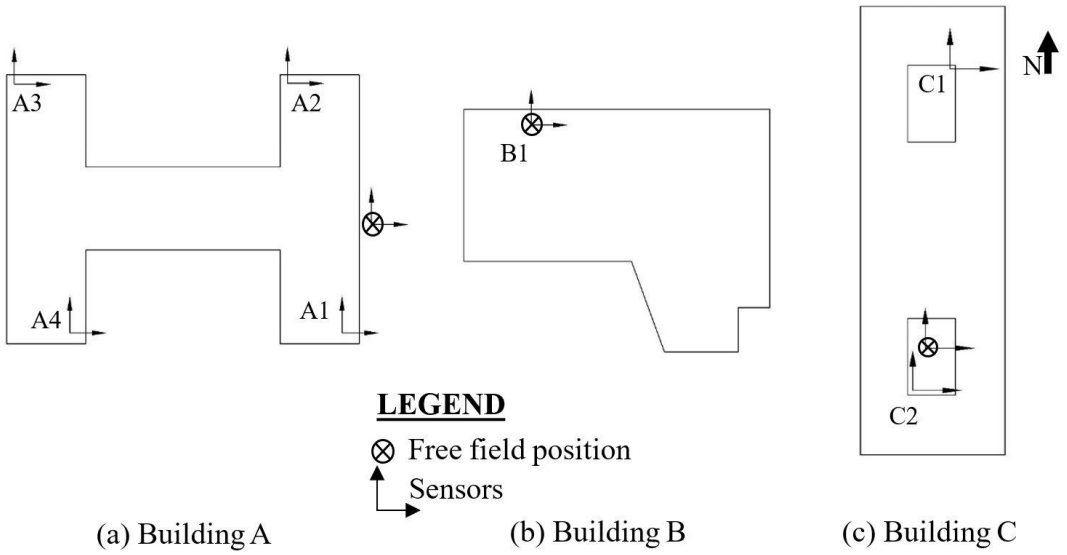

Figure 3.4: Sensor layout for instrumented adjacent buildings

3.3 Data Acquisition

Vibration data was collected from the adjacent structures and respective free field positions using high sensitivity seismic uniaxial piezoelectric accelerometers before, during and after the implosion of Cather and Pound halls. The measurement range of the piezoelectric accelerometers is ± 5 g with a frequency range of 0.06 – 450 Hz. The vibration data was recorded at a sampling rate of 2048 Hz which was later downsampled to 256 Hz to reduce the computational complexity during processing of the vibration data. This gives a Nyquist sampling rate of 128 Hz. The frequency range of interest for this experimental study is approximately 0.1 Hz to 50 Hz considering the response at free field positions and within the adjacent structures. Given that 128 Hz is more than twice the required 50 Hz, this sampling rate is sufficient for this study. The ambient vibration data obtained from Building A and Building B before the implosion of Cather and Pound halls has been used in the system identification of the two adjacent structures. The system

identification of Building A and Building B is detailed in Chapter 4. Similarly, the acceleration response data obtained from the three adjacent structures and their respective free field positions during the event of blast and collapse has been discussed in time domain and frequency domain in Chapter 5 and Chapter 6. The acceleration response data used in Chapter 5 and Chapter 6 were filtered using a bandpass Butterworth filter of order 3 between 0.1 Hz and 50 Hz. The MATLAB script used for the Butterworth filter is shown in Figure 3.5.

```
 [N,~] = size(Acc);
fcutin=0.1;
fcutoff=50;
forder=3;
[b,a] = butter(forder,[fcutin fcutoff]/(0.5*fs),'bandpass');
[h1,f1] = freqz(b,a,N,'whole',fs);
df = 1/(dt*N);
    f = 0:df:(N-1)*df;
 parfor i=1:length(channels)
        acc_filt(:,i)=filtfilt(b,a,Acc(:,i));
         acc_filt(:,i) = acc_filt(:,i)-mean(acc_filt(:,i));
 end
```

Figure 3.5: Filtering using Butterworth filter

Although each of the nearby structures had more than two sensors installed, only two horizontal sensors from the most prominent location at the roof level of each structure is selected to show a comparison of acceleration responses between these structures. Among the sensors selected, the sensors for Building A are located on the southeast corner of the roof, the sensors for Building C are located on the southwest corner at the roof level, and the sensors for Building B are located on the northwest corner at the third-floor level (see Figure 3.4).

CHAPTER 4 – SYSTEM IDENTIFICATION OF ADJACENT STRUCTURES

4.1 System Identification: An Overview

System identification of a structure refers to the estimation of modal parameters of a structure based on mathematical models of recorded responses of the structure under excitations (Chaudhary et al. 2000). The structural parameters in system identification of a structure usually include the modal parameters like frequency, damping ratio, and mode shapes which are key in defining the dynamic properties of a structure. In recent years, system identification has gained strong attention within structural engineering disciplines like structural health monitoring and calibration of the finite element model (FEM). One of the prime motivations of system identification of structure is to quantify the dynamic characteristics of the structure that could help to assess the current state of the structure and evaluate the safety of structure against the excitation due to wind and earthquake motions. System identification methods broadly include two methods: input-output and output-only for the estimation of modal parameters. Input-output methods are accompanied by forced vibration tests in a structure where input excitation forces are measured simultaneously with the recorded responses within the structure. Forced vibration tests in system identification of structures include the development of frequency response function (FRF) from the output acceleration responses relating to the measured input-excitation forces in the structure. While forced vibration tests (with large eccentric mass shakers) can be performed for input-output measurements, the input measurements may not always accurately represent the excitation forces; especially in complex

structures (Ren et al. 2004). This has given rise to output-only system identification techniques where modal parameters are based only on the measured output response of a structure. Output-only modal analysis is often referred as operational modal analysis (Peeters and De Roeck 2001). Operational modal analysis technique relies on the measured output responses of structures in its operating condition through ambient vibration testing. Ambient vibration tests refer to the measurement of the response of a structure to an ambient source of excitations like wind and live loads.

4.2 Examples of Case Studies using Ambient Vibration Tests

Ambient vibration testing is a widely used output-only dynamic testing method to reliably estimate the modal parameters of several structures. The ambient vibration tests are relatively inexpensive compared to forced vibration tests and allow the testing of full-scale structures without interrupting its service condition. The simplicity of the instrument setup, which usually includes only lightweight instruments make the ambient vibration testing a convenient testing method for system identification of structures. The ambient vibration tests have been conveniently used in the system identification of large structures like Golden Gate Bridge in San Francisco, California (Abdel-Ghaffar and Scanlan 1985) to determine the modal parameters (effective damping, mode shapes, and frequencies). Likewise, Ren et al. (2004) evaluated Roebling suspension bridge over the Ohio River using ambient field testing under natural excitation to estimate the dynamic properties of the bridge. The dynamic properties of the bridge were used to update and modify the finite-element model (FEM) of the bridge. Ren et al. (2004) have also shown a comparative study between the experimental modal analysis using the ambient

vibration testing and analytical modal analysis on a steel arch bridge located in Tennessee. Further, ambient vibration testing is also widely used to obtain the dynamic properties of buildings. Jaishi et al. (2003) used an ambient vibration method under wind-induced excitation to obtain the real dynamic properties of three multi-tiered masonry temples located in Nepal. The estimated dynamic properties were used to validate the finite element models of those temples. Some other examples of the ambient vibration testing used in system identification of structures are Fatih Sultan Mehmet (Second Bosporus) suspension bridge (Brownjohn et al. 1992), Kap Shui Mun cable-stayed bridge (Chang et al. 2001), multi-story office towers (Brownjohn 2002).

4.3 Instrumentation and Data Processing

Ambient vibration data were obtained from two adjacent structures: Building A and Building B prior to the event of implosion and collapse of Cather and Pound Halls. The instrumentation setup that was used to record the response of adjacent structures to blast and collapse was also used to obtain the ambient vibration of the adjacent structures before the blast and collapse of Cather and Pound halls. The details regarding the sensor setup that was used in this experimental study are discussed in Section 3.2.

The obtained ambient vibration data for Building A and Building B were pre-processed prior to the system identification of these buildings. First, a Hampel filter was applied to the acceleration response data to remove the outliers due to voltage spikes. The response data was filtered with a bandpass filter using the FIR filter in MATLAB. The response data for Building A was filtered within a frequency band between 3.5 Hz and 10 Hz. The MATLAB script used to apply the FIR filter to the ambient vibration data of

Building A is shown in Figure 4.1. Likewise, the response data for Building B was filtered between a frequency of 0.5 Hz and 6 Hz using the same approach as used for filtering of ambient vibration data for Building A. The limits of the bandpass filter for Building A and Building B were selected to highlight the first two modes of each structure based on the preliminary analysis of the ambient vibration data in the frequency domain. The total duration of ambient vibration data used in the system identification of Building A and Building B was 9.8 hours and 4.9 hours respectively. The durations of ambient vibration data for each of these buildings were selected based on the resolution of the peaks of interest and the signal to noise ratio in the frequency domain of the ambient vibration data. A longer duration of ambient vibration data was used for Building A since the preliminary analysis of ambient vibration data in frequency domain indicated a very low signal to noise ratio.

The number of sensors at the roof level available for system identification of Building B was limited to two. The frequency domain of the ambient vibration response for Building B along the E-W and N-S direction indicated clear peaks in each direction. Hence, peak-picking method was used which was adequate to obtain the first two natural frequencies of Building B represented by the first peak in frequency domain along the E-W and N-S direction. However, a Curve Fitted Frequency Domain Decomposition (CFDD) was employed in the system identification of Building A since the ambient vibration data had a very low signal to noise ratio and the frequency domain of the ambient vibration data did not yielded any clear peaks. The system identification methods used to estimate the natural frequencies of Building A and Building B are further described in Section 4.4 and Section 4.5.

```
[N,~] = size(Acc);
    forder=4096*10;  %FIR Filter Order
    fcutin=3.5;      %FIR Filter Cutin Frequency
    fcutoff=10;       %FIR Filter Cutoff Frequency
    dt = 1/fs;
    df = 1/(dt*N);
    f = 0:df:(N-1)*df;
    fnyq = fs/2; % Nyquist frequency
    b1 = fir1(forder,[fcutin/fnyq fcutoff/fnyq],'bandpass');
    [h1,f1] = freqz(b1,1,N,'whole',fs);
    parfor i=1:length(channels)
        Acc(:,i) = filter(b1,1,Acc(:,i));
        Acc(:,i) = Acc(:,i)-mean(Acc(:,i));
    end
```

Figure 4.1: Application of bandpass filter to ambient vibration data using FIR filter

4.4 System Identification: Building A

The natural frequencies of Building A were estimated using the frequency domain technique within Operational Modal Analysis known as Curve Fitted Frequency Domain Decomposition (OMA-CFDD). As discussed in the earlier section, OMA is an output-only system identification technique which allows the estimation of modal parameters of the structure while the structure is in its operation. OMA is a system identification technique that relies on the measurement of the output response of a structure assuming that the input ambient excitation is stochastic and often technically referred as white noise (Peeters and De Roeck 2001). Peeters and De Roeck (2001) have presented a review of frequency domain techniques and time domain techniques that can be used to estimate modal parameters through OMA.

The ambient vibration response data obtained for Building A indicated a very minimum level of ambient excitation such that the signal-to-noise ratio was very low. The response data contained significant noise contamination. OMA-FDD allows the estimation of modal frequencies with higher accuracy even if the output response is

highly contaminated with noise (Brincker et al. 2000). Brincker et al. (2000) includes the detail on OMA-FDD technique where the spectral density function matrix is divided into auto spectral density functions using Singular Value Decomposition (SVD) such that each auto spectral density function is a single-degree of freedom system representing an individual mode. The individual modes are then manually picked in the frequency domain to obtain the modal frequencies and the mode shapes. In OMA-CFDD technique, the auto spectral density function is curve fitted with an SDOF curve, and the mode shape is estimated using the Modal Assurance Criterion (MAC) discussed under OMA-EFDD (Operational Modal Analysis-Enhanced Frequency Domain Decomposition) (Jacobsen et al. 2007). The first two modal frequencies obtained for Building A using OMA-CFDD is summarized in Table 4.1.

Table 4.1: System identification of Building A (OMA-CFDD)

Modes	Frequency [Hz]	Complexity [%]	Motion
Mode 1	4.074	0.398	Translation predominantly E-W
Mode 2	4.892	2.513	Translation predominantly N-S

The complexity percentage indicated in Table 4.1 represents whether the mode shape is a real or imaginary. 0 % complexity refers to a Real Mode, and 100 % refers to an Imaginary Mode. Figure 4.2 shows the singular values of spectral densities of the ambient vibration response of Building A along with the modal frequencies obtained from OMA-CFDD. The three curves in Figure 4.2 indicate spectra of singular values of output acceleration measurements from three sensors out of four sensors used for OMA-CFDD in modal analysis software Artemis Modal (ARTeMIS 2019). Only 3 singular values have been shown in Figure 4.2 since three sensors can fully explain the modal

identification for the shown frequency range. The curve fitted auto spectral density function for the two modes obtained using a modal analysis software ARTeMIS Modal is shown in Figure A.1 and Figure A.2 in Appendix A.

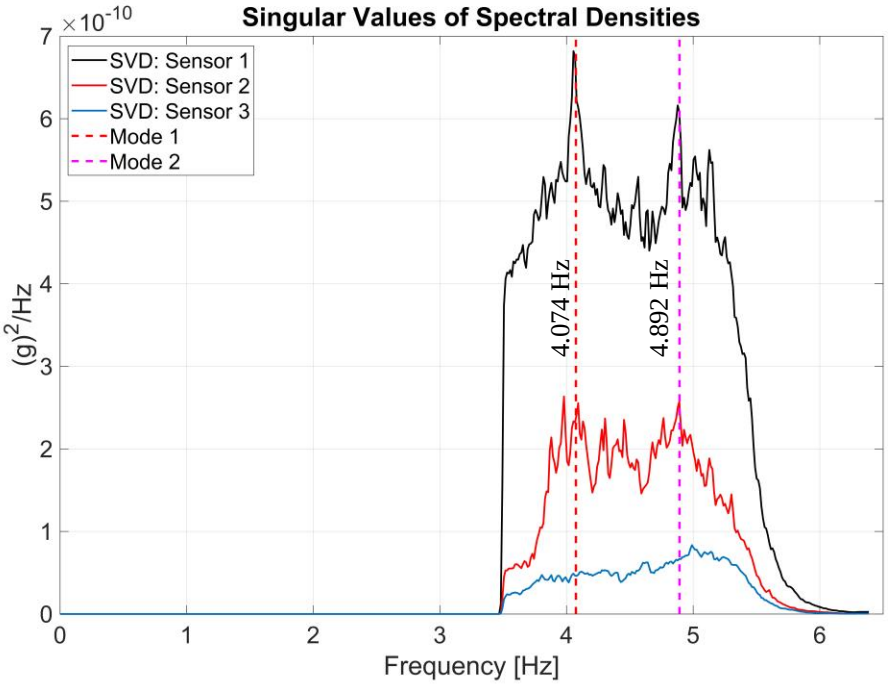

Figure 4.2: System identification of Building A: OMA-CFDD *(*SVD-Single Value Decomposition)*

Building A has an I shaped configuration, and a preliminary operational modal analysis of the I-shaped configuration indicated that each flange of I-shape of Building A behaved independently of each other. The modal frequencies shown in Table 4.1 are based on the ambient vibration data obtained from four sensors located on the east side of Building A. A review of the floor plans provided for Building A also showed evidence that the flanges and web of I-shaped configuration of Building A were not structurally interconnected. Hence the modal frequencies presented in Table 4.1 represent only the natural frequencies of the east flange of Building A.

4.5 System Identification: Building B

The system identification of Building B was done using the ambient vibration data obtained from two sensors located on its third floor. Peak-picking method in frequency domain was used to estimate the modal frequencies of Building B. Peak-picking is a frequency-domain technique within OMA and one of the simplest modal analysis techniques for ambient vibration tests (Peeters and De Roeck 2001). With the number of available sensors for system identification being limited to just two, the estimation of the modal frequencies along two directions (N-S and E-W) relied on the peaks observed in the averaged power spectral density plots. The power spectral density (Bendat and Piersol 1993) plots were generated for each window length of 60 s of acceleration response and then averaged to obtain an averaged power spectral density. The peak-picking in the obtained power spectral density is shown in Figure 4.3. The estimated modal frequencies for Building B are summarized in Table 4.2.

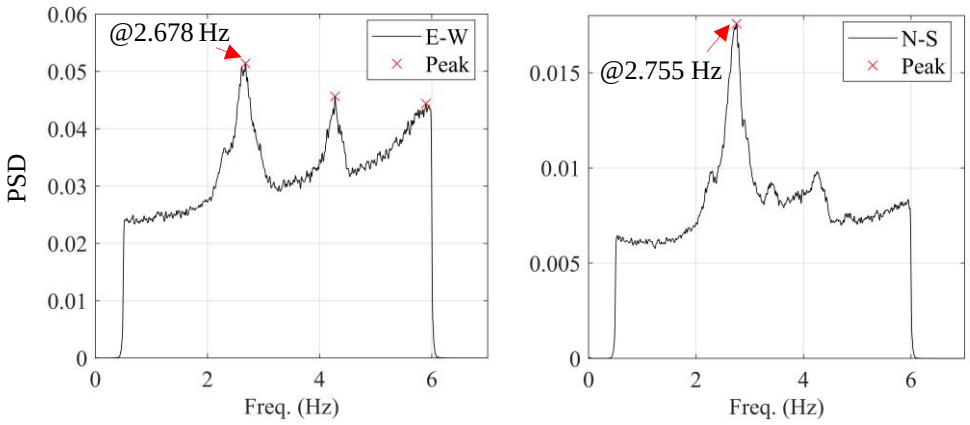

Figure 4.3: System identification of Building B using peak-picking

Table 4.2: System identification of Building B using peak-picking

Mode	Frequency [Hz]	Direction
Mode 1	2.678	E-W
Mode 2	2.755	N-S

4.6 Application to this research

The natural frequencies obtained for Building A and Building B through system identification techniques have been used to calibrate the finite element model of these two buildings presented in Chapter 7. The obtained natural frequencies would also be used to draw key insights over the response of Building A and Building B to the blast and collapse sequences. Further, this would help to differentiate the nature of observed structural responses to blast-induced ground motions and collapse-induced ground motions. An understanding of the natural frequencies of a structure would also be key to distinguish any observed higher modal response during the event of the blast and collapse. The significance of the estimated modal frequencies of Building A and Building B is described within the discussions presented in Chapter 6 and Chapter 7.

CHAPTER 5 – EXPERIMENTAL OBSERVATIONS: ADJACENT STRUCTURES

5.1 An Overview

Response data obtained from the free field positions and from within the adjacent structures during the event of implosion and collapse of Cather and Pound Halls are presented in the time domain and frequency domain in this chapter. Key ground motion parameters of the response data obtained from free field positions were calculated to study the variation of ground motions at three free field positions that are discussed in Chapter 3. Likewise, a comparison between the response at free field position due to the blast and collapse sequence is presented to understand as well as differentiate the effects of blast and collapse-induced ground motions. The detailed instrumentation setup used to collect the response data is presented in Chapter 3. The response data obtained before and after the event of the implosion is primarily used in the interpretation of responses in Chapter 6 and for the calibration of numerical models of the adjacent structures which is detailed in Chapter 7.

5.2 Response Data

This section aims to characterize the response data collected during the implosion and collapse in terms of the key ground motion parameters as well as present the acceleration response recorded at three adjacent structures and their respective free field positions. The ground motion parameters used here include Peak Ground Acceleration

(PGA) and 5-95% Significant Duration based on Arias Intensity ($Duration_{5-95}$) (Bommer and Pereira 1999). Each of the acceleration time history at three free field positions show a distinct acceleration response to the blast followed by a distinct acceleration response to the collapse with a well-defined time gap of approximately 1.3 s in between the two distinct responses. The correspondence of these two distinct response sequences was verified using the synchronized video and audio data of the implosion obtained during this experiment.

Table 5.1 gives the PGA and $Duration_{5-95}$ for the total acceleration response at three free field positions as well as uses the same ground motion parameters to define the acceleration response sequences for blast and collapse. The PGA at three free field positions shows a significant variation depending upon the direction and location of the sensor as well as depending upon whether the response corresponds to the blast or collapse sequence of the response data. At FF. Pos. 1, PGA ranges from 0.047 g in the E-W direction to 0.077 g in the vertical direction. FF. Pos. 1 also recorded the highest acceleration response among all the free field positions which is reasonable to the fact that FF. Pos. 1 is at closest proximity to the demolition site. Likewise, at FF. Pos. 2, N-S sensor shows a PGA of 0.018 g and the E-W sensor shows a PGA of 0.008 g. Provided that FF. Pos. 2 is further from the demolition site when compared to FF. Pos. 1, the observed response at these two free field positions indicate an exponential decay of the motion's amplitude with respect to the distance. Likewise, FF. Pos. 3 being furthest from the demolition site shows noticeably minimal acceleration response among all the free field positions. Both E-W sensor and N-S sensor at FF. Pos. 2 show PGAs of the order of 0.002 g. Further looking at Table 5.1, FF. Pos. 1 being closest to the demolition site has

the least significant duration and FF. Pos. 3 being furthest from the demolition site has the greatest significant duration. FF. Pos. 3 lies on the ground floor of a 13-story structure and the highest significant duration at FF. Pos. 3 can be attributed to the longer period of excitation of the 13-story structure. The response within this adjacent structure is further detailed in the following sections.

Table 5.1: Peak ground acceleration (PGA) and significant duration based on Arias Intensity ($Duration_{5\text{-}95}$) at three free-field positions

		Ground Motion Parameters					
Position	Direction	PGA [g]			$Duration_{5\text{-}95}$ [s]		
		Blast	Collapse	Total	Blast	Collapse	Total
FF. Pos. 1	North	0.045	0.061	0.061	3.163	4.906	11.505
	East	0.026	0.047	0.047	3.537	5.090	11.560
	Vertical	0.024	0.077	0.077	3.354	5.483	6.155
FF Pos. 2	North	0.014	0.018	0.018	3.920	4.688	10.095
	East	0.008	0.013	0.013	4.235	5.179	10.300
FF. Pos. 3	North	0.001	0.002	0.002	5.935	7.320	7.730
	East	0.001	0.002	0.002	5.265	6.185	6.540

Figure 5.1 shows the acceleration time histories for three transverse sensors at FF. Pos. 1. Similarly, Figure 5.1 shows a comparison of acceleration time histories for E-W sensor and N-S sensor at all three free field positions. A finite time separation between the blast and collapse response is distinct in all the time histories shown in

Figure 5.1 and Figure 5.2. This time separation after the blast response and before the onset of the collapse response can be related to the redistribution of the loads within the reinforced concrete structure due to the failure of individual columns within the structure. When comparing the blast response and collapse response for each of the time histories at three free field positions, it is distinctive that the collapse response dominates the overall acceleration response in terms of the PGA as well as the significant duration.

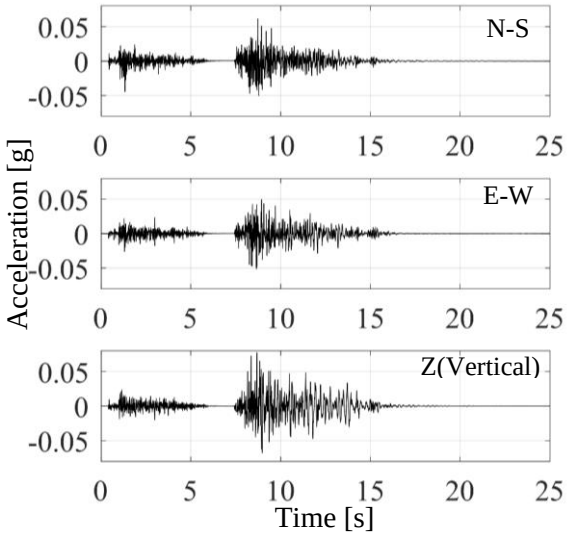

Figure 5.1: Acceleration time history – FF. Pos. 1

The acceleration responses that were recorded within the three adjacent structures are shown in Figure 5.3. Both Building A and Building B show much higher acceleration response compared to the minimal acceleration response recorded at Building B. The higher responses for Building A and Building B is reasonable since both of these buildings are located very near to the demolition site. While E-W sensors for Building A and Building B show a comparable peak acceleration of 0.073 g and 0.079 g respectively, the E-W sensor for Building C shows a much lower peak of 0.004 g. However, Building A and Building B show a significant difference in acceleration response in N-S direction

with peak acceleration of 0.080 g in N-S sensor of Building A and a peak acceleration of 0.022 g in N-S sensor of Building B. Such variation of peak responses between Building A and Building B could be attributed to the difference between two structures in terms of geometric configuration as well as the materials used in the construction of these two buildings. Building C being the furthest from the demolition site shows an acceleration response of noticeably longer duration which further justifies the statement that the higher significant duration of FF. Pos. 3 can be attributed to the structural response of Building C.

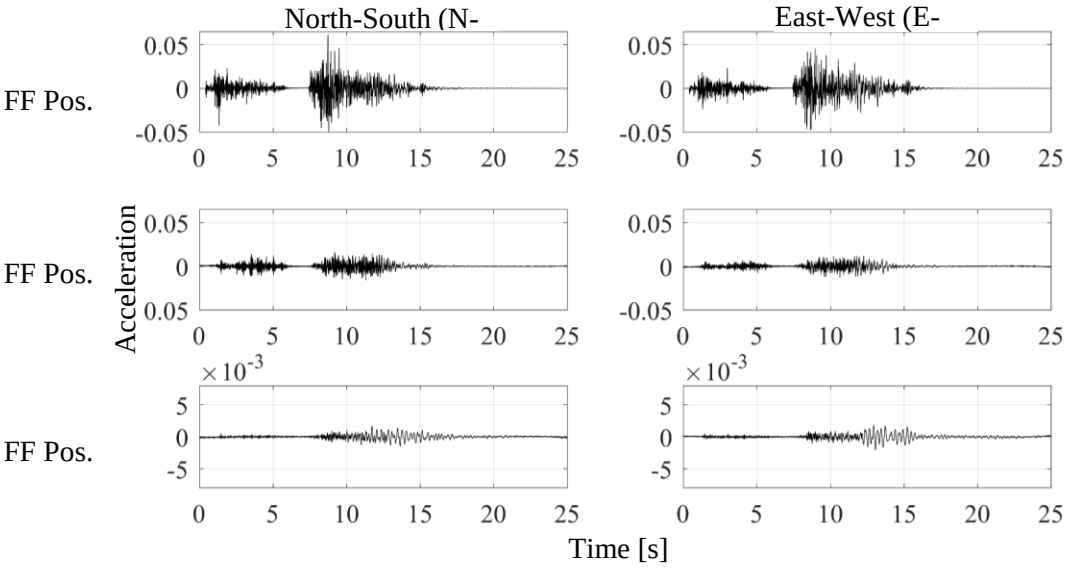

Figure 5.2: Acceleration time histories at three free-field positions (Note: Y-axis of FF. Pos. 3 is plotted to a different scale)

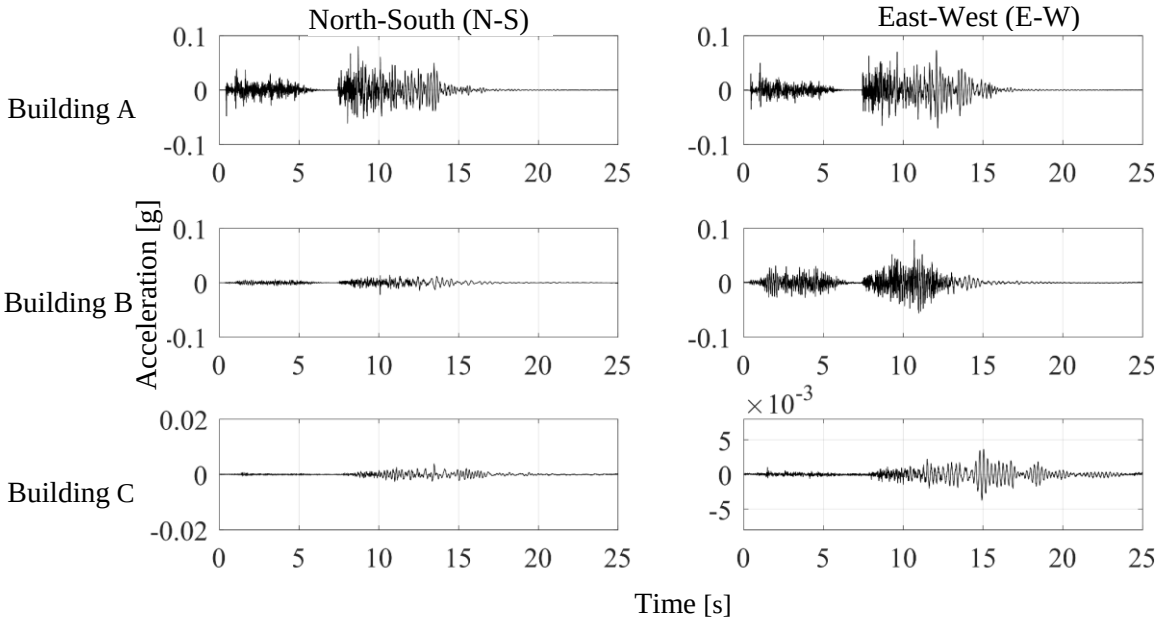

Figure 5.3: Acceleration time histories for sensors at roof level in Building A, Building B and Building C (Note: Y-axis of Building C is plotted to a different scale)

5.3 Analysis of Response Data

The response data presented in Section 5.2 is analyzed in the frequency domain using elastic response spectrum in this section. Spectral acceleration values are computed in the elastic response spectrum for a range of natural periods of interest. Spectral acceleration refers to the peak absolute acceleration of a damped single-degree of freedom system with a certain natural period, when subjected to ground motions. Spectral acceleration is equal to peak ground acceleration for a natural period of zero. An elastic response spectrum has been prepared for the acceleration responses obtained from the free-field and from within the building, where a damping value of 5 percent of the critical damping is assumed.

Figure 5.4 shows spectral accelerations (S_a) for three transverse sensors at FF. Pos. 1 where the vertical sensor has the highest value of peak S_a (0.24 g). Likewise, E-W sensor shows a peak S_a of 0.19 g and N-S sensor shows a peak S_a of 0.18 g. The higher spectral acceleration for the vertical sensor indicates a higher magnitude of vertical motion due to the collapse of the buildings following the blast. The elastic response spectrum for vertical sensor at FF. Pos. 1 also shows a plateau of S_a peaks within the period of 0.02 s – 0.03 s. Whereas, the S_a peaks for E-W and N-S sensors are concentrated in the lower period region less than 0.2 s. A key observation in these response spectrums is a pulse-like behavior where a pulse-like response is observed around the period of 0.5 s for the vertical sensor and a similar pulse-like response is observed around the period of 0.4 s for the N-S sensor. The video footage obtained during the demolition and collapse of Cather and Pound shows that both the buildings exhibit a progressive collapse between the floors having uniform heights with the overall collapse leaning in N-S direction. The overall progressive collapse of two building being primarily oriented in N-S direction further corroborates the pulse-like behavior observed in N-S and vertical sensor in Figure 5.4.

Figure 5.5 shows the comparison of elastic response spectrums at three free field positions. FF. Pos. 1 shows a higher spectral acceleration response among all three free field positions since FF. Pos. 1 is closest to the demolition site. As expected, FF. Pos. 3 being the furthest free field position from the demolition site shows the least spectral acceleration of all. Likewise, FF. Pos. 1 and FF. Pos. 2 have peaks dominating over higher frequency range when compared to the spectral acceleration peaks that spread out within a comparatively lower frequency range for FF. Pos. 3. The high-frequency

response of the FF. Pos. 1 and FF. Pos. 2 could be attributed to the fact that these sites are nearer to the demolition site. Likewise, since FF. Pos. 3 is tied to a tall structure, the overall structural response must have dominated the peak responses at FF. Pos. 3 resulting in the peaks at lower frequency range.

Figure 5.6 shows the spectral acceleration responses along N-S and E-W direction at the roof level of Building A, Building B and Building C. As expected, the peak spectral acceleration responses at the roof of all three buildings are higher than the peak spectral responses at their respective free field positions. The peaks of spectral acceleration responses at each building represent the natural period at which the building was being excited as a result of the blast and collapse. Among the three buildings, Building C shows a distinct response along E-W direction with a dominant period of around 0.3 s which could be due to the response of this 13-story building being dominated by the excitation of one of its higher modes. The variability of spectral acceleration response between three buildings can be attributed towards the distance of the building from the demolition site, geometric configuration and system properties of each building and the location of sensors within the building.

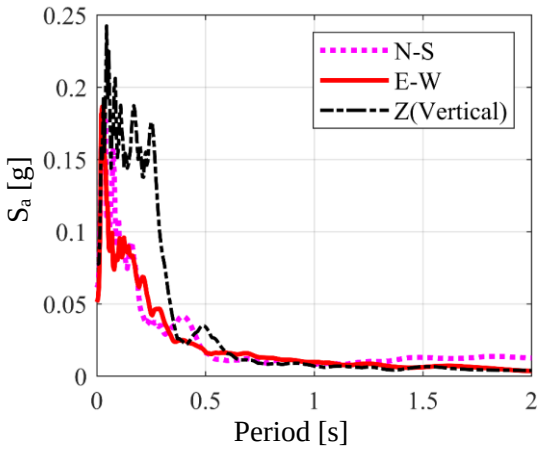

Figure 5.4: Spectral acceleration at FF. Pos. 1 (ξ= 5 % critical)

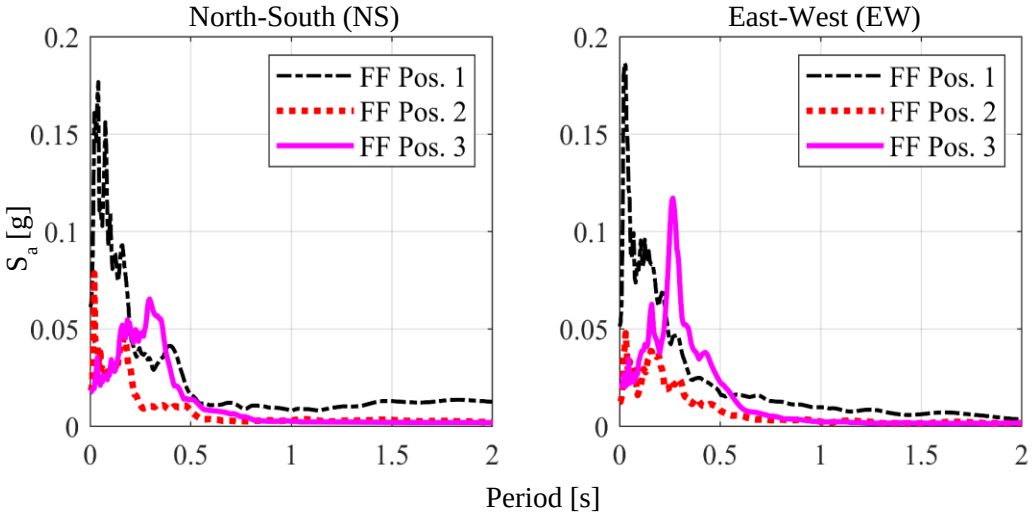

Figure 5.5: Spectral acceleration of the three free-field positions ((ξ= 5 % critical) ***(Note: S_a for FF. Pos. 3 is scaled by factor of 10)***

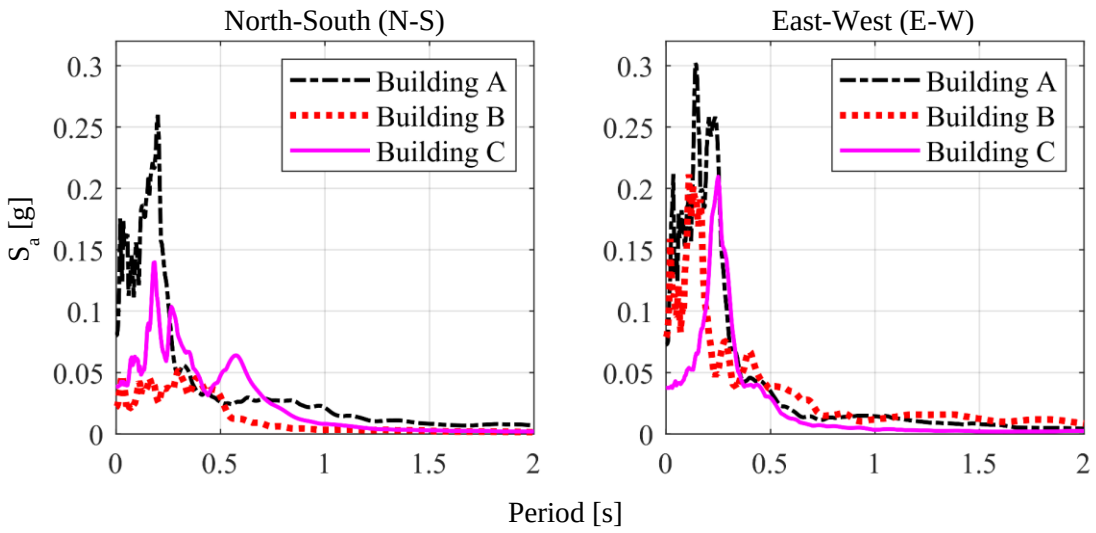

Figure 5.6: Spectral acceleration of the roof level sensors of the adjacent buildings ((ξ= 5 % critical) *(Note: S_a for Building C is scaled by a factor of 10)*

5.5 Response Data: Blast vs. Collapse Sequence

The clear distinction between the response towards the blast and the collapse sequence of Cather and Pound Halls is a prominent feature of this experimental study. This section aims to break down the total acceleration response at FF. Pos. 1 due to blast and collapse and analyze the response observed in terms of the elastic response spectrum. A typical acceleration time history shown in

Figure 5.1 shows an initial response to the blast loads that was applied to the individual columns of Cather and Pound which is then followed by a time gap of approximately 1.3 which can be attributed towards the time taken for the redistribution of the loads within Cather and Pound before the initiation of the collapse sequence. The response towards the collapse sequence is distinct in all the acceleration time histories of Figure 5.1 to Figure 5.3.

Table 5.1 shows a comparison of key ground motion parameters between the blast and collapse sequence at three free field positions. It is evident that the collapse sequence dominates the total response in terms of PGA as well as the significant duration at all three free field positions. At FF. Pos. 1, the vertical sensor shows the highest PGA of 0.077 g when considering the collapse sequence only which can be attributed to the dominant vertical motion due to the progressive collapse of Cather and Pound Halls. However, when considering the blast sequence at FF. Pos. 1, the highest PGA of 0.045 g is observed at N-S sensor which indicates a higher intensity of blast load distributed along N-S direction. Likewise, the significant duration at all three free field positions is higher for collapse sequence when compared to the blast sequence. This can be supported with the observation of a typical time history in

Figure 5.1 where the total duration of response to collapse sequence is higher than the total duration of response to blast sequence. Further, FF. Pos. 3 shows a higher significant duration than all other free field positions for both blast and the collapse sequence which relates back to our previous discussion of FF. Pos. 3 being tied to a 13-story structure such that the response at FF. Pos. 3 is saturated by the response of its structure. The higher significant duration at FF. Pos. 3 is also evident in the spectral acceleration shown in Figure 5.5.

The comparison between the blast and collapse sequence is further demonstrated in Figure 5.7 which shows spectral accelerations for both blast and collapse sequence at FF. Pos. 1. The spectral acceleration for the blast sequence at FF. Pos. 1 shows very high-frequency Sa peaks located within the period of less than 0.1 s. However, the spectral acceleration for the collapse sequence shows a plateau of peaks which extend up to a

period of 0.4 s typically observed in vertical sensor at FF. Pos. 1. Likewise, the spectral acceleration response spectrum for the collapse sequence also shows the pulse-like behavior within the period of 0.3s and 0.6s. This further supports the previous discussion that the pulse-like behavior is a contribution of the collapse sequence.

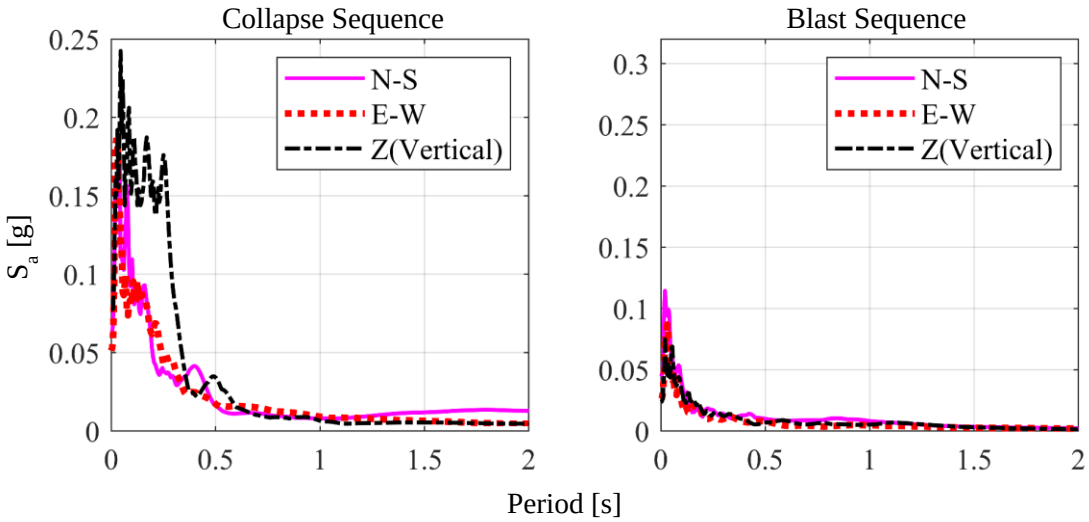

Figure 5.7: Spectral acceleration at FF. Pos. 1 (ξ= 5 % critical)

5.6 Conclusions

Key observations made from the response data obtained from the three adjacent structures and the conclusions made from the analysis of the response data are summarized as follows:

1. The collapse sequence of the demolition dominates the responses recorded within three adjacent structures and their respective free field positions.

2. A pulse-like behavior around the period of 0.4 s and 0.5 s can be observed vertically as well as horizontally (N-S) in the elastic response spectrum at FF. Pos. 1. This can be attributed towards the progressive collapse of the Cather and Pound halls being predominantly oriented along N-S direction.
3. A very minimal response is observed at FF. Pos. 3 when compared to FF. Pos. 1 and FF. Pos. 2. This indicates an exponential decay of the blast and collapse-induced ground motion's amplitude with respect to the distance.
4. Although Building C is furthest from the demolition site, the building shows a relatively longer period of response when compared to Building A and Building B.
5. Blast-induced ground-motions show a very high-frequency content, but a very low amplitude compared to relatively lower frequency content and higher amplitude of collapse-induced ground motions.

CHAPTER 6 – INPUT-OUTPUT STUDY: BLAST VS. COLLAPSE SEQUENCE

6.1 An Overview

This chapter presents a detailed comparison between the ground motions due to blast and collapse sequences and the response of the buildings to these ground motions through an input-output study. The key differences between the blast and collapse-induced ground motions were discussed in terms of time histories, elastic response spectra, and scalar ground motion parameters in Chapter 5. While the blast and collapse-induced ground motions have different durations, the elastic response spectra of the ground motion at FF. Pos. 1 (closest to the implosion site and Building A) shown in Figure 6.1 indicate that these two sequences also vary in terms of their frequency content. Since the total response of the adjacent structures during the implosion and progressive collapse is dominated by the collapse sequence in terms of amplitude, a separate study of the structural response to both the blast and collapse sequences is presented to better understand and differentiate the response of the adjacent structures towards these two different ground motions. In addition, an input-output study of the response of the adjacent structures to the blast and collapse sequences can elucidate if sources other than the ground motion contributed to the building's response (e.g., air wave from the blast).

The input-output study presented in this chapter looks specifically at the spectral acceleration amplification observed at the roof level of both Building A and Building B. Building C is not included in this study due to the relatively low amplitude of response,

in comparison to the other two buildings which were in much closer proximity to the implosion. In concert with the system identification results for both buildings, the difference between the elastic response spectra at the roof of the building and at the ground will be indicative of the influence of the air wave on the structure's response.

6.2 Ground Motions: Blast vs. Collapse Sequence

The key differences in the characteristics of the ground motions at the site nearest to the implosion (FF. Pos. 1) due to both the blast and collapse sequences is presented in Section 5.5. As part of that presentation, elastic response spectra were generated to understand the primary frequency content of both the blast and collapse sequences. It can be seen that the blast sequence predominantly included frequency content above 10 Hz (0.1 s); however, the ground motion due to the collapse sequence included a much broader frequency range with an approximately lower limit of 2 Hz (0.5 s).

Figure 6.1 shows the elastic response spectra for both the blast and collapse sequences in the N-S and E-W directions for the ground motion at FF. Pos. 2 (ground level of Building B). These spectra evidence similar frequency content to that observed at FF. Pos. 1 (just outside Building A and nearest to the implosion site), including higher frequency content for the blast sequence (lower limit of 10 Hz (0.1 s) and broader frequency content for the collapse sequence (lower limit of 2 Hz (0.5 s)). The collapse sequence also shows evidence of pulse-like behavior around 0.45 s in the N-S direction for both free field positions. This makes sense considering the pattern of the progressive collapse, which consisted of sequential impacts due to regularly-spaced floors with the collapse progressing in the N-S direction.

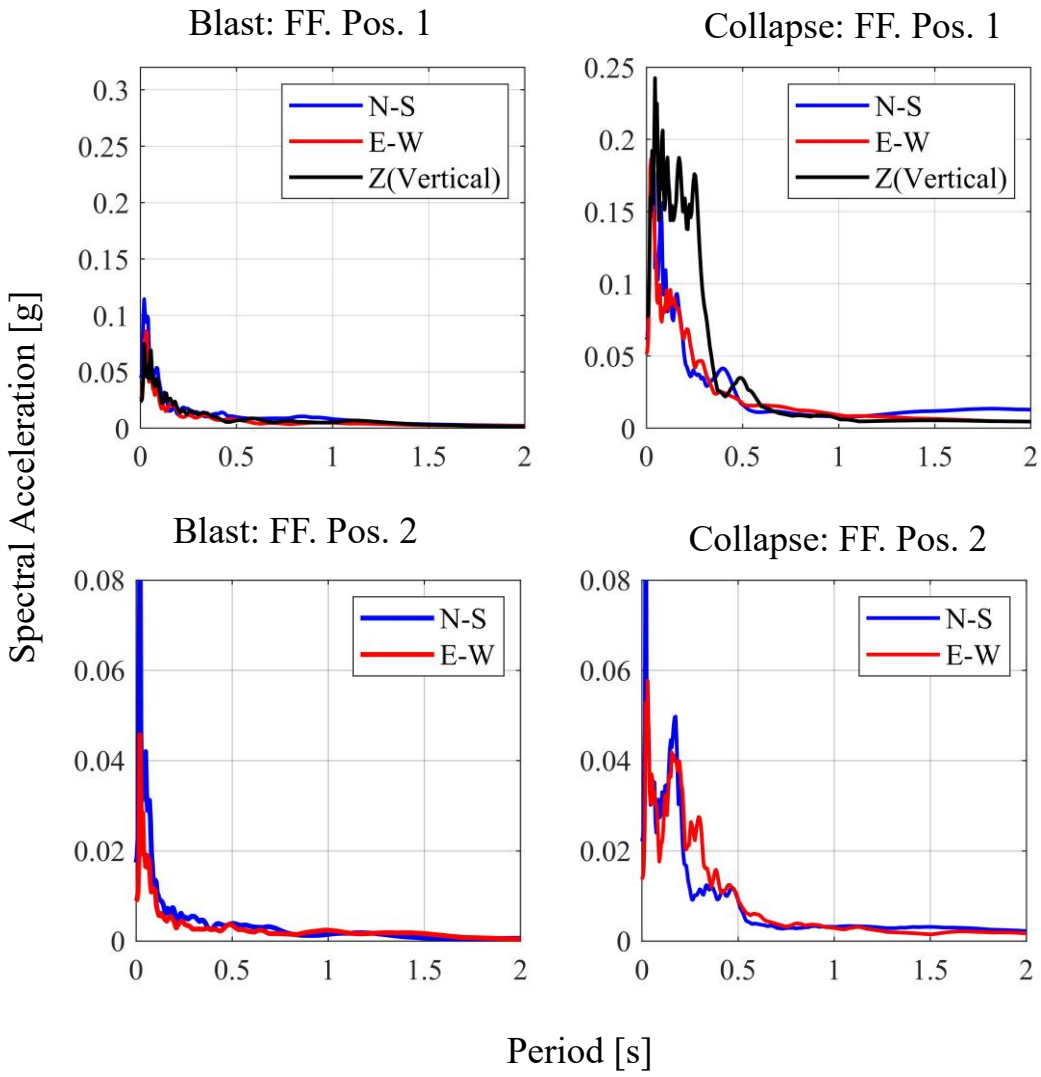

Figure 6.1: Elastic response spectrum at FF. Pos. 1 and FF. Pos. 2: Blast vs. Collapse (ξ= 5 % critical)

6.3 Input-Output Study: Building A

Building A is a very key site to study the effect of the airblast wave due to its proximity to the implosion. Moreover, FF. Pos. 1 was installed in the free field and not attached within Building A, which leads to more realistic information regarding the blast and collapse-induced ground motions. This section includes a comparison of the ground

motion with the response of Building A, followed by a study of the spectral acceleration amplification observed at the roof of Building A. The overall goal of the study is to gain an understanding of the causality of the ground motion to the structures' responses. If the frequency content evidenced at the roof level of the buildings does not agree with the input ground motion in light of the system identification results, alternative excitation sources such as the air wave could be significant.

6.3.1 Building Response vs. Ground Motion

This section forms a base of discussion for spectral amplification observed at the roof of Building A that is discussed in section 5.3.2.Figure 6.3 shows a comparison of the elastic response spectrum for the motion recorded at the roof level of Building A and for the ground motion recorded just outside this structure (FF. Pos. 1) for the blast sequence only in both horizontal directions. The elastic response spectrums for the ground sensor along N-S and E-W direction as shown in Figure 6.3 show that the ground response was dominated by short-period.

While the E-W sensor on the roof of Building A shows an amplified response in the high-frequency region (below 0.1 s), the N-S sensor shows a lower spectral acceleration (attenuation) in the same high-frequency region compared to that of the ground in the same direction. At very high frequencies of excitation relative to the building's natural frequency, the building is not anticipated to evidence substantial response based on fundamental structural dynamics. In addition, the high frequency blast-induced ground motions originate from a point-source and travel towards the building.

Therefore, the entire structure may not be subjected to the same ground motion, which would be a function of the excitation wavelength.

The shear wave velocity in the upper 30 m of the soil is 300 m/s (USGS 2019),

Using,

$Velocity\ (V) = Frequencey\ (f)\ x\ Wavelength\ (\lambda)$

For a half cycle excitation of a 50 Hz signal,

$f = 50\ Hz$

$V = 300\ m/s$

Implies,

$$\lambda = \frac{V}{f} x \frac{1}{2} = \frac{300\ m/s}{50\ Hz} x \frac{1}{2} = 3\ m$$

This implies,

Wavelength of 10 Hz signal = 15 m

Wavelength of 5 Hz signal = 30 m

An interpretation of the half cycle wavelength required to uniformly excite the structure at its base is presented in Figure 6.2. This indicates that the half-cycle wavelength of the structure should be at least equal to or greater than the width of the structure in order to uniformly excite the structure at its base on both ends (A and B). While the blast will generate compressional, shear, and surface waves, this analysis considers only the shear waves as they are the primary contributor to ground motion and

building shaking. Given that the width of the building is 30 m, the frequency of the excitation should be as low as 5 Hz in order to uniformly excite the building. Likewise, using the same above-mentioned relationship of velocity, frequency and wavelength, it can be obtained that the frequencies above 20 Hz (0.05 s) would not uniformly excite the structure and a relatively low structural response is expected. This is clearly identified in the short period range of the N-S spectra. Similar findings were found by Dowding et al. (2018), in which the effect of mining blasts was evaluated against nearby structures. On the other hand, the E-W sensor on the roof at Building A shows an amplified response in the high frequency or short-period region. This likely indicates that the building is responding not only to the ground motion but also to the air wave from the blast.

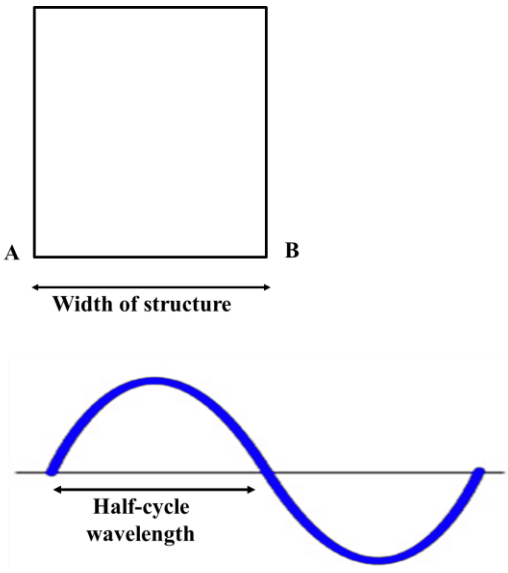

Figure 6.2: Half cycle wavelength and width of structure

While the building responded quite differently in the N-S and E-W directions in the high-frequency range, the building evidenced an amplified response in the periods

greater than 0.1 s in both directions. However, the response spectra do not show significant amplification in the vicinity of the natural periods (0.20 s and 0.24 s). This is likely simply related to the lack of significant excitation in that frequency range. This is studied further through amplification spectra in the next section.

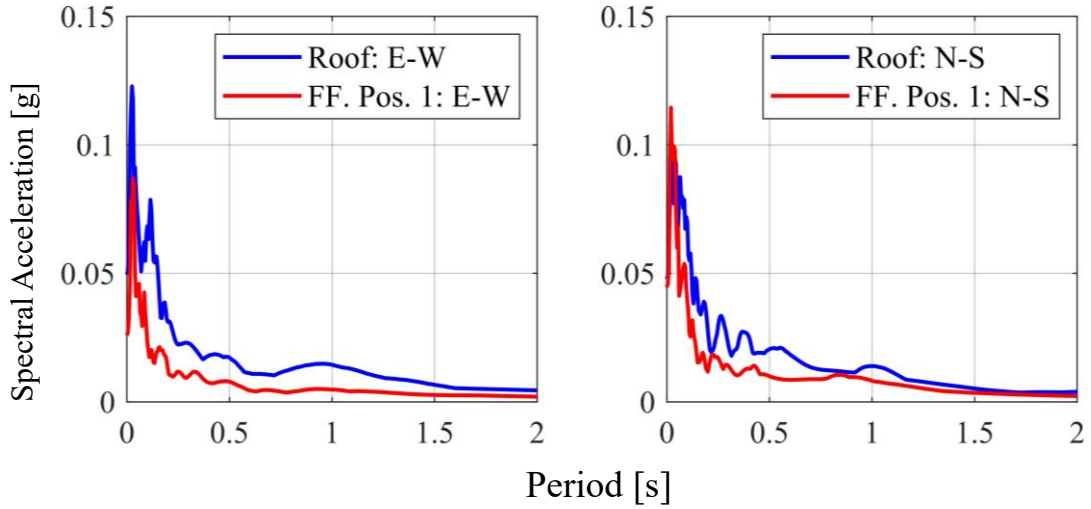

Figure 6.3: Elastic response spectrum at Building A and FF. Pos. 1 for blast sequence (ξ= 5 % critical)

Figure 6.4 shows the comparison between the elastic response spectrum for the collapse induced ground motions at FF. Pos. 1 and the structural response observed on the roof of Building A during the collapse sequence. The system identification for Building A indicates a fundamental period of 0.25 s along E-W direction and a natural period of 0.20 s along N-S direction. The elastic response spectrum on the roof along both directions is dominated with peaks near the natural period of the structure in that direction. The E-W sensor shows two prominent spectral peaks at the period of 0.24 s and 0.15 s. While the spectral peak at 0.24 s for E-W sensor is indicative of the structure responding at its natural period of the vibration along E-W direction, the spectral peak at

0.15 s is indicative of the structure responding in a higher mode along E-W direction. Likewise, the peak spectral acceleration for N-S sensor is located at the natural period of 0.20 s which is a clear indication of the structure responding in its natural period of vibration along N-S direction. The lower frequency content of the collapse-induced ground motion is also evident on Figure 6.4 where a notable spectral acceleration response can be observed up to a period of 0.4 s.

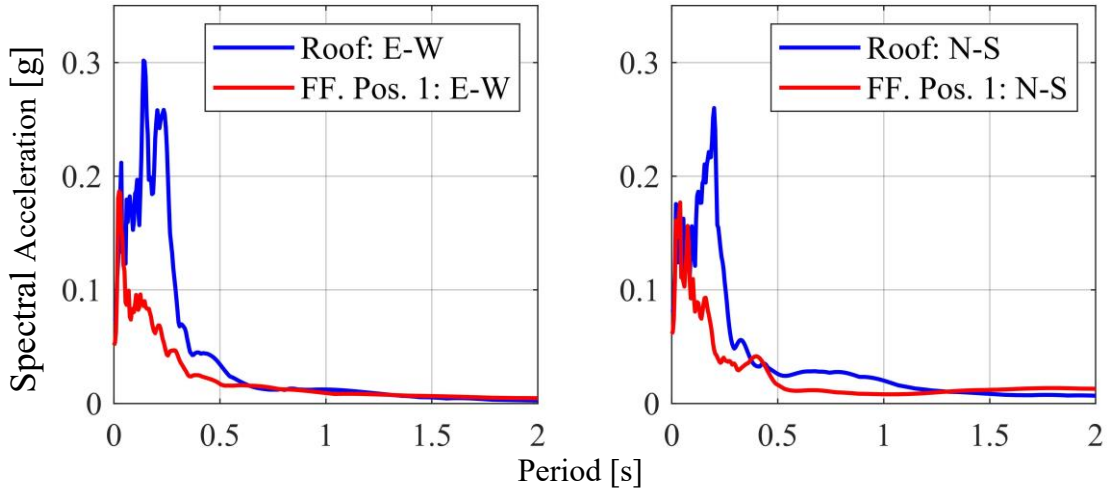

Figure 6.4: Elastic response spectrum at Building A and FF. Pos. 1 for collapse sequence (ξ= 5 % critical)

6.3.2 Amplification of Ground Motion: Blast vs. Collapse

The spectral acceleration amplification observed in the roof of Building A with respect to the blast and collapse induced ground motions at FF. Pos. 1 is shown in Figure 6.5. The amplification is computed simply as the ratio of the spectral acceleration at the roof to that at the ground. It is noted that both the ground motion and the structural response due to the blast sequence included very low values of spectral acceleration in the period range above 0.5 s, and these amplification values should not be considered

significant. The spectral amplification for the blast sequence along the E-W direction shows a peak with amplitude 4 at a period of 0.115 s which refers to a frequency of 8.683 Hz. However, no clear peak can be noted in the spectral amplification along N-S direction of the structure for the blast sequence. Building A is oriented such that the east façade is directly exposed to the implosion, while the north and south sides are not exposed to the implosion. The higher exposure of Building A on the east side and the unique higher order response of the building along E-W direction for the blast sequence shows a strong indication towards the possible dominant effect of the airblast wave on the response of the structure along the E-W direction.

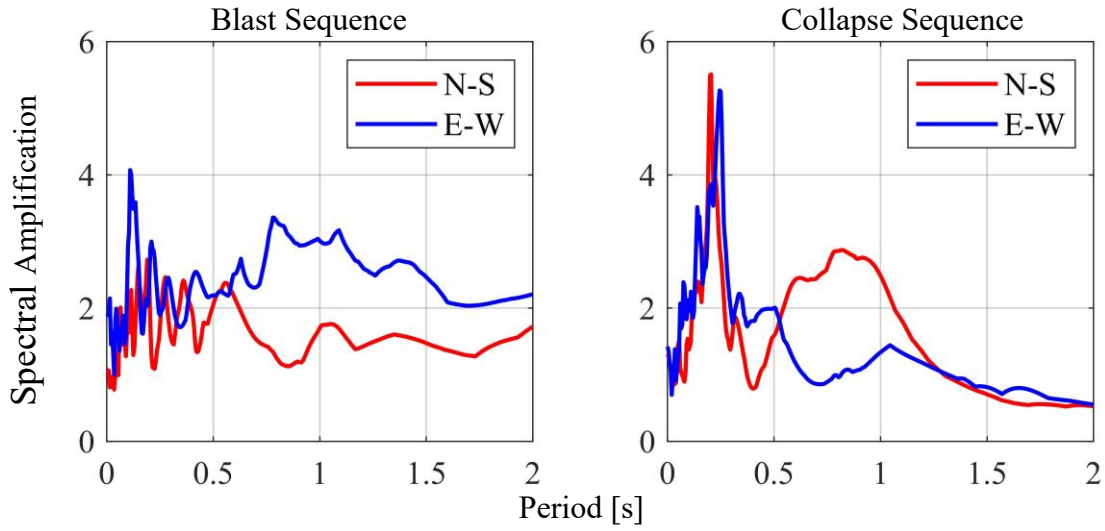

Figure 6.5: Spectral amplification at the roof of Building A (ξ= 5 % critical)

A structure usually shows a high amplification towards ground motion when the structure responds closer to its natural period of vibration. In Figure 6.5, the spectral amplification for the E-W sensor at Building A for the collapse sequence shows a major peak of the order of 5.3 at the period of 0.25 s which is also the natural period of the building along E-W direction. Likewise, the spectral acceleration amplification along N-S

direction shows a dominant spectral amplification of the order of 5.5 at 0.20 s which is the natural period of Building A along N-S direction. Similar to the case for the blast sequence, the spectral acceleration for the collapse sequence in both directions had very low values in the period region greater than approximately 0.5 s. Therefore, the fluctuation and peaks in this region are not considered significant.

6.4 Input-Output Study: Building B

Building B is the second closest adjacent structure in terms of the proximity to the demolition site. Although the free field position for Building B was not attached to the real ground, an input-output study of this building can provide key insights over the effect of the airblast wave in the overall structural response of Building B during the blast sequence. A comparative study of the response at the FF. Pos. 2 and the response at the roof of Building B is presented in terms of the elastic response spectrum for both blast and collapse sequence of the response. Likewise, key observations are discussed based on the spectral amplification observed within Building B with respect to FF. Pos. 2 during sequences of blast and collapse.

6.4.1 Response at Structure vs. Response at Ground: Blast vs. Collapse

Figure 6.6 compares the spectral acceleration at the roof of Building B with the spectral acceleration at FF. Pos. 2 due to the blast sequence. The response to the blast sequence shows a similar trend as observed in the FF. Pos. 1 and at the roof of Building A. Particularly, the E-W sensor at the roof of Building B shows an amplified response when compared to the response at the FF. Pos. 2 along the E-W direction during the blast

sequence. The elastic response spectrum for the E-W sensor on the roof of Building B during the blast sequence shows a dominant response at the period of 0.125 s and another prominent spectral response at a very low period of 0.03 s. These two periods refer to the frequency of 8 Hz and 33.33 Hz respectively. The amplified response of the structure at a very high frequency is unique for a structure responding to blast-induced ground motions with high frequency. This unique response of the building along E-W direction was also observed in the response of Building A to the blast sequence. The fact that Building B also has very high exposure of its west façade towards the demolition site shows a strong indication of the structure predominantly responding along E-W direction to the airblast wave in constructive interference with the response to the blast-induced ground motion along the E-W direction.

On the contrary, Figure 6.6 shows an attenuated response at the roof of Building B along the N-S direction for the blast sequence. While the elastic response spectrum along N-S direction at FF. Pos. 2 shows a spectral peak of 0.069 g at a very high frequency of 50 Hz, the roof sensor along N-S direction shows a de-amplified spectral peak of 0.029 g at frequency of 7.8 Hz. The de-amplified response along N-S direction can be related to the discussion made in the previous section for Building A comparing the wavelength of the motion to the footprint dimensions of the building. In this case, the width of Building B is approximately 36 m in the N-S direction. Similarly, assuming a shear wave velocity of 300 m/s, frequency content greater than 16.7 Hz (0.06 s) would not uniformly excite the base of the structure. Therefore, it implies that the building will not respond significantly in the short-period range. This behavior strongly correlates with the attenuated structural response of Building B along N-S direction to the blast

sequence. Moreover, this further corroborates that the unique amplified response of Building A and Building B to blast sequence at high-frequency region is likely due to secondary effects other than the blast-induced ground motion, such as the blast-induced air wave.

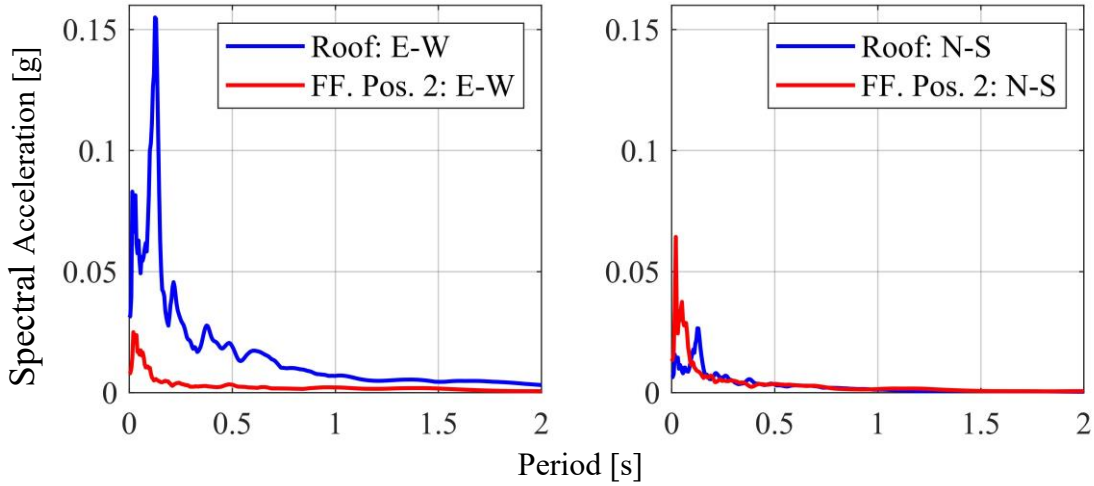

Figure 6.6: Elastic response spectrum at Building B and FF. Pos. 2 for blast sequence (ξ= 5 % critical)

Figure 6.7 shows a comparison of the elastic response spectrum at the roof of Building B and at FF. Pos. 2 along N-S and E-W directions for the collapse sequence. It is evident from the figure that the response to collapse sequence at the FF. Pos. 2 and at the roof of Building B contains a much broader frequency content with frequency as low as 2 Hz (0.5 s) when compared with the respective responses to the blast sequence. The E-W sensor at the roof of Building B shows an amplified response with respect to FF. Pos. 2 with major peaks at periods of 0.17 s and 0.11 s, which indicates a higher order structural response for a structure with a fundamental natural period of 0.384 s along E-W direction. The N-S sensor at the roof of Building B shows much lower spectral peaks

than E-W sensor for the collapse sequence. In the short-period range, there is effectively no amplification of the ground motion, as expected given that the natural period is approximately 0.4 s. However, it is evident that the natural frequency of the structure in this direction is excited due to the amplification present in the vicinity of 0.4 s.

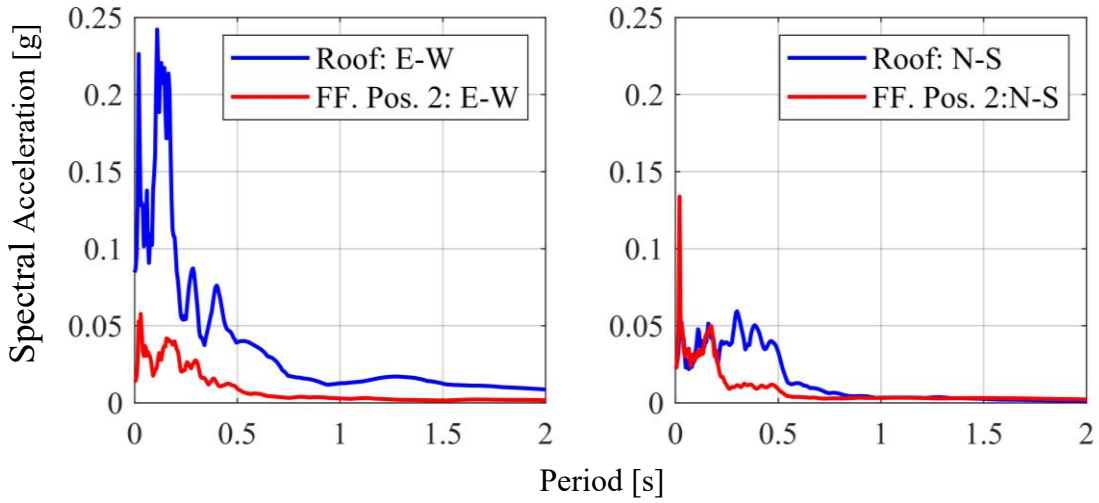

Figure 6.7: Elastic response spectrum at Building B and FF. Pos. 2 for collapse sequence (ξ= 5 % critical)

6.4.2 Amplification of Ground Motion: Blast vs. Collapse

Figure 6.8 demonstrates the spectral acceleration amplification observed in the third floor of Building B with respect to FF. Pos. 2 for both blast and collapse sequence. A very high spectral amplification of the order of 29 is observed in the roof of Building B along E-W direction for blast sequence. The collapse induced ground motion along E-W direction in FF. Pos. 2 has higher PGA and greater duration than blast-induced ground motion along the same direction. However, the spectral amplification observed along E-W direction in the roof for collapse sequence is only of the order of 10 which is much

lower when compared with the spectral amplification along E-W direction for the blast sequence. A very high spectral amplification along the E-W direction at a period of 0.125 s (0.8 Hz) indicates that the blast-induced ground motion was dominated by a frequency content much higher than 8 Hz. This also indicates that the blast-induced ground motion had a very low value on the lower period region of the spectrum. Likewise, a lower value of amplification observed along E-W direction for collapse sequence indicates a much broader band of frequency content in the acceleration response at FF. Pos. 2. Figure 6.7 shows that the dominant spectral response at FF. Pos. 2 for collapse sequence is extending beyond 5 Hz towards a lower frequency region of the elastic response spectrum.

Regardless of the order of amplification observed in blast and collapse sequence, a prominent higher order structural response at a period less than 0.2 s is visible for both sequences of ground motion. The spectral amplification along N-S direction for the collapse sequence shows a de-amplification for a low period region of the spectrum but shows distinct amplification around the period of 0.39 s. This distinct amplification is close to the natural period of 0.37 along N-S direction for Building B. However, the amplification along the E-W direction shows a higher order amplification with scattered peaks around both higher and lower region of the response spectrum.

The E-W sensor at the third floor of Building B shows more prominent peaks of higher order amplification for blast sequence when compared with the higher order amplification for collapse sequence along the same direction, see Figure 6.8. Although the collapse-induced acceleration response at FF. Pos. 2 was more dominant than the blast-induced acceleration response, the prominence of higher order amplification for

blast sequence along the E-W direction does indicate towards secondary effects in the response of Building B during the blast sequence. Likewise, as discussed for Building A, Building B also has its west façade directly exposed to the demolition site. This could be the reason that the airblast wave generated during the blast wave could have made a significant impact on the response of Building B along the E-W direction during the blast sequence. A constructive interference of the response of Building B to the airblast wave and the response of the building to the blast-induced ground motions along E-W could have resulted in the higher order response amplification of Building B along E-W direction during the blast sequence.

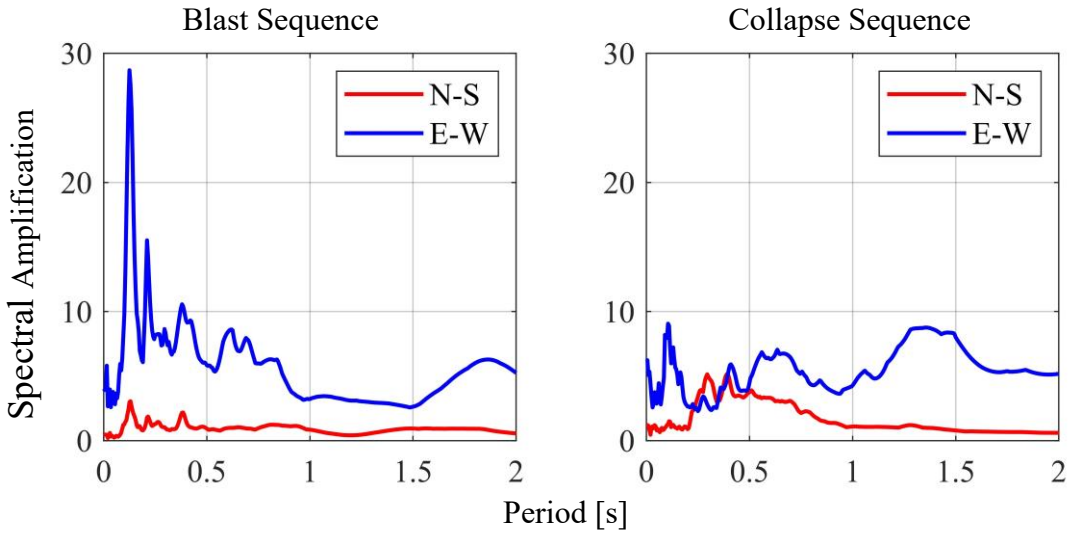

Figure 6.8: Spectral amplification at the roof of Building B (ξ= 5 % critical)

6.5 Conclusion

Key observations and conclusions made from the input-output study at Building A and Building B are summarized as follows:

1. While the blast-induced ground motions show a very high-frequency content with a lower bound of approximately 10 Hz, the collapse-induced ground motions show much broader frequency content with frequency as low as 2 Hz.
2. Both Building A and Building B show an attenuated response to blast sequence along N-S direction in the low period (high frequency) range lower than approximately 0.1 s. This is due, in part, to the short wavelengths of the blast-induced ground motions, which were not long enough to uniformly excite the structures.
3. Building A and Building B show an amplified response to the blast sequence along the E-W direction, which is unexpected given the relatively high-frequency content of the blast sequence compared to the natural frequency of the buildings. This is indicative of the contribution of the blast-induced air wave to the building's responses.

CHAPTER 7 – NUMERICAL MODELING

7.1 An Overview

The experimental results discussed in Chapter 5 and Chapter 6 encompass the effects due to a wide range of parameters that could influence the response of the adjacent structures during the implosion. Two of these key parameters discussed in this thesis are the soil domain and the airblast wave. The soil domain beneath the structure can have a major influence on the ground motions and the structural response to ground motions. Chapter 2 presents studies about how the interaction between the soil and structure can affect the response of structures to ground motions. Likewise, Chapter 6 discusses about the possibility of the effect of airblast wave in the response of the adjacent structures during the blast sequence.

Building A and Building B are numerically modeled with fixed base assumptions in this chapter using LS-DYNA (LSTC 2019). The fixed base assumption refers to a lumped mass model restrained at its base for all degree of freedoms where the effect of the flexibility of the soil domain on the foundation level is neglected. This refers to a perfectly rigid foundation assumption and enables the separation of the effects of the soil domain as well as the effect of the airblast wave in the observed responses of Building A and Building B during the blast and progressive collapse of Cather and Pound Halls. The acceleration responses obtained from the FF. Pos. 1 and FF. Pos. 2 are used as input ground motions in the numerical model of Building A and Building B, respectively. This helps to provide key insights regarding the effect of the soil domain over the fixed base responses of Building A and Building B. Furthermore, the observed responses from the

numerical model also help to distinguish possible higher mode effect of the airblast wave discussed in Chapter 6.

7.2 Overview of LS-DYNA Modeling Approach

LS-DYNA is a robust finite element and multi-physics program capable of modeling complex structural and soil systems (LSTC 2019). LS-DYNA uses an explicit time integration method as its primary solver to perform the finite element analyses. The finite element program has a wide variety of elements like four node tetrahedron and eight node elements, two node beam elements, truss elements, rigid bodies, etc. that can be used based on the analysis requirements. The program also has a large collection of contact types and material models to choose from depending upon the types and applications of the numerical model. The numerical models for Building A and Building B are constructed and analyzed in LS-DYNA. The developed models are summarized below in terms of geometry, element, materials, contact and loading as follows:

a) Geometry

Building A and Building B have been modeled using the lumped-mass model approach where both of these structures have been approximated by a single line element equivalent to the height of the structures, and a lumped mass on the roof level.

b) Element

The line element used in the numerical models of Building A and Building B is a two-node Belytschko beam element with a section defined under the keyword

SECTION_BEAM in LS-DYNA. The lumped mass at the top of each line element is defined using the keyword ELEMENT_MASS in LS-DYNA.

c) Materials

The line element used in Building A has been defined with an elastic concrete property under the keyword MAT_ELASTIC. The elastic concrete properties used are summarized as follows:

- Mass density = 0.0868 lb-s^2/in
- Young's modulus of elasticity = 3.6 E06 psi
- Poisson's ratio = 0.2

Likewise, the line element used in Building B has been defined using an elastic steel property under the keyword MAT_ELASTIC. The elastic steel properties used are summarized as follows:

- Mass density = 7.33e-4 lb-s^2/in
- Young's modulus of elasticity = 3.0e07 psi
- Poisson's ratio = 0.3

d) Contact

The base node of the Building A and Building B is defined as a fixed support with the keyword BOUNDARY_SPC_NODE. The node at the roof level is restrained to allow only translations along the x and y directions.

e) Loading

The two orthogonal ground motion time histories along north and east direction obtained from FF. Pos. 1 and FF. Pos. 2 were applied at the base node of numerical model for Building A and Building B along y and x direction respectively. The ground motions were prescribed to the base node using the keyword BOUNDARY_PRESCRIBED_NODE in LS-DYNA.

f) Damping

A constant value of damping for a frequency range of 0.1 Hz to 50 Hz was applied on the numerical models for Building A and B using the keyword DAMPING_FREQUENCY_RANGE. This keyword provides approximately constant damping that is independent of frequency over a range of frequencies prescribed by the user. Building A is an older masonry structure and a damping value of 10 % of critical was assumed. Likewise, a constant damping value of 8 % of the critical damping was assumed for the numerical model of Building B. The assumption of these damping values are based on the visual inspection of the preliminary comparison between the numerical response and the experimental response.

7.3 Calibration of Numerical Models

A detailed discussion on the system identification of Building A and Building B is presented in Chapter 4. The numerical models for Building A and Building B were calibrated to match closely with natural periods of these two structures obtained from the system identification. The keyword IMPLICIT_EIGENVALUE was used in LS-DYNA to obtain the eigenvalues and natural frequencies of numerical models for Building A and Building B. An iterative procedure was used for both numerical models to match their

natural periods with results obtained from the system identification in Chapter 4. For Building A, the size of the section of line elements and the values of lumped masses were modified to obtain the desired natural period of the numerical model. The natural periods obtained from the calibrated model for Building A is presented in Table 7.1 along with natural periods obtained from the system identification (System ID.). Similar to the numerical model of Building A, the size of the section of the line elements and the value of lumped mass were modified to obtain the desired natural period of the numerical model. Then natural periods of the calibrated model of Building A are presented in Table 7.2 along with the natural periods obtained from System ID.

Table 7.1: Numerical Model vs. System Identification (Building A)

Modes	Direction	Period [s] (Numerical Model)	Period [s] (System ID.)
Mode 1	E-W	0.246	0.245
Mode 2	N-S	0.205	0.204

Table 7.2: Numerical Model vs. System Identification (Building B)

Mode	Direction	Period [s] (Numerical Model)	Period [s] (System ID.)
Mode 1	E-W	2.69	2.68
Mode 2	N-S	2.76	2.76

It should be noted that while using the keyword DAMPING_FREQUENCY_RANGE in LS-DYNA, there is a reduction in the frequency of the numerical model. The reduction in the frequency of the numerical model was adjusted by increasing the stiffness of the numerical model. The stiffness of the numerical

model was increased in such a way that the numerical model shows a dominant response at its natural frequency along N-S and E-W directions when subjected to a white noise excitation.

7.4 Results: Building A

The ground motions obtained from FF. Pos. 1 were prescribed to the fixed base of the numerical model of Building A to obtain the acceleration response at the roof level. The numerically obtained acceleration responses along the E-W and N-S directions are presented in the time and frequency domains. A comparison is presented in both time and frequency domains between the numerical response and the experimentally obtained response at the roof level of Building A.

7.4.1 Numerical Response vs. Experimental Response in Time Domain

The numerical model of Building A is a two-degree of freedom (2DOF) model calibrated for the first two natural frequencies. The experimentally obtained response from the roof level of Building A was filtered between the frequency range of 3.05 to 6.11 Hz for comparison with the simplified 2DOF numerical model. The selected upper and lower bound of the frequency range of the filter is 25 % below and 25 % above the first two natural frequencies of the building. A finite impulse response (FIR) filter of the order of 2100 was used to obtain the filtered experimental response of Building A. The MATLAB script of the filter is shown in Figure 7.1.

The comparison of peak accelerations at the roof between the numerical response and the experimental response are presented in Figure 7.2. It is fairly evident in Figure

7.2 that the 2DOF model shows more comparable response to the low-frequency collapse sequence of the ground motions than the high-frequency blast sequence of the ground motions along both E-W and N-S directions.

```
fcutin=3.05;
fcutoff=6.11;
forder=2100;

    [N,~] = size(Acc);
    dt = 1/fs;
    df = 1/(dt*N);
    f = 0:df:(N-1)*df;
    fnyq = fs/2; % Nyquist frequency
    [b1,a1] = fir1(forder,[fcutin1/fnyq fcutoff1/fnyq],'bandpass');
    [h1,f1] = freqz(b1,a1,N,'whole',fs);
parfor i=1:length(channels)
 acc_filt(:,i) = filtfilt(b1,a1,Acc(:,i));
 acc_filt(:,i) = acc_filt(:,i)-mean(acc_filt(:,i));
end
```

Figure 7.1: MATLAB script used in filtering using FIR filter

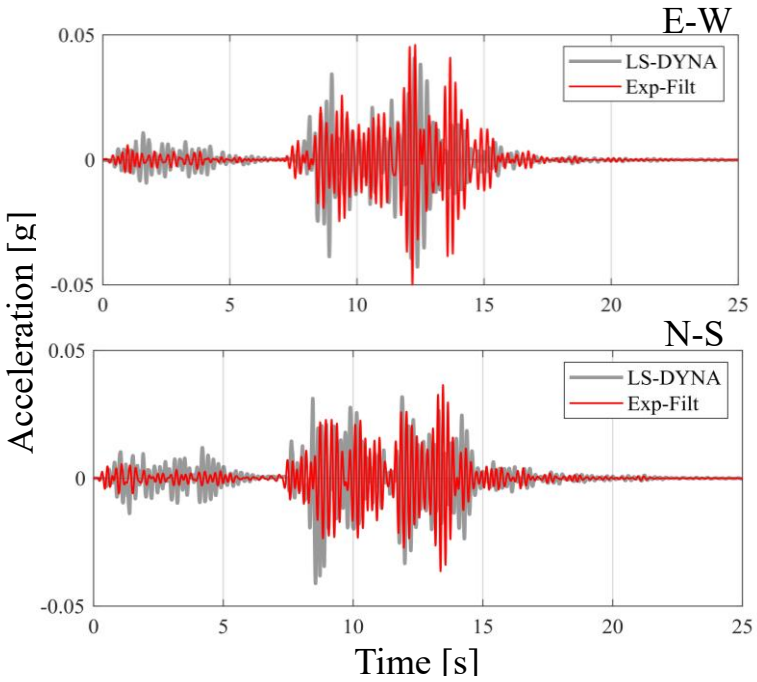

Figure 7.2: Comparison of acceleration time history: LS-DYNA vs. Exp-Filt *(*Exp-Filt: Experimental response filtered between 3.05 to 6.11 Hz)*

Table 7.3 and Table 7.4 show the comparison of peak acceleration values between the numerical response and the filtered acceleration response along E-W and N-S directions. While the percentage difference of peak accelerations for the numerical and filtered experimental response is 16.5 % for the collapse sequence along E-W direction, the percentage difference of the compared peak accelerations for blast sequence is 45.3 %. A similar trend is observed in the N-S direction as well. This is an expected behavior of the 2DOF numerical model, where the numerical model shows a better prediction of the experimental response dominated by frequency near the first two natural periods of the numerical model. In addition to the inability to replicate the higher mode response, the blast-induced air wave could have further excited the building during the blast sequence, which is not incorporated into the numerical model.

Table 7.3: Peak acceleration values: LS-DYNA vs. Exp-Filt along E-W*(*Exp-Filt: Experimental response filtered between 3.05 to 6.11 Hz)*

E-W				
Response Data	Blast		Collapse	
	Peak Acc. [g]	% Diff	Peak Acc. [g]	% Diff
Numerical	0.011	45.280	0.043	16.546
Exp-Filt	0.006		0.050	

Table 7.4: Peak acceleration values: LS-DYNA vs. Exp-Filt along N-S*(*Exp-Filt: Experimental response filtered between 3.05 to 6.11 Hz)*

N-S				
Response Data	Blast		Collapse	
	Peak Acc. [g]	% Diff	Peak Acc. [g]	%Diff
Numerical	0.014	56.418	0.041	11.314
Exp-Filt	0.006		0.036	

7.4.2 Numerical Response vs. Experimental Response in Frequency Domain

The roof acceleration responses obtained from the numerical analysis of Building A is analyzed in the frequency domain with elastic response spectrums in terms of both blast and collapse sequences. The elastic response spectrums of the numerical responses along E-W and N-S directions have been compared with the corresponding elastic response spectrums at the roof of Building A obtained from the experimental response.

7.4.2.1 Blast Sequence

Figure 7.3 shows the comparison of elastic response spectrums of the numerical and filtered experimental response along E-W and N-S direction during the blast sequence. Figure 7.3 is also overlaid with the elastic response spectrum of the original experimental response at the roof. As expected, the numerical model being a 2DOF model does not show any distinct response at higher modes other than the first two modes along E-W and N-S. The numerical response for the blast sequence is similarly dominated by peak responses at natural periods along E-W and N-S directions. Table 7.5 shows a summary of spectral accelerations for numerical response and experimental response at the natural period along E-W direction. Likewise,

Table 7.6 shows spectral acceleration for numerical response and experimental response at natural period along N-S direction. The comparison of the elastic response spectrum of the blast sequence shows a higher spectral acceleration for the numerical

response than the experimental response. The experimental response indicates a drastically reduced response in comparison to the numerical model. Table 7.5 and

Table 7.6 both indicate a very high percentage difference of the spectral accelerations between the numerical response and experimental response compared at the first two natural periods of Building A along E-W and N-S direction. The high percentage difference of the spectral accelerations can be largely attributed to the small values of spectral acceleration evidenced in both the experimental and the numerical responses. In addition, the numerical model greatly simplifies the excitation to the structure, where the numerical model is subjected to ground motion only while the experimental structure was subjected to ground motion and airblast wave.

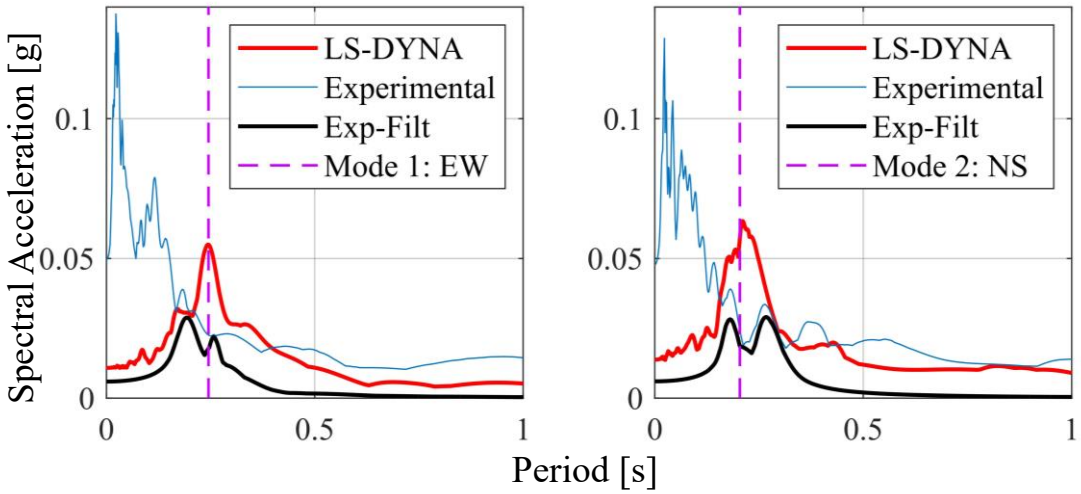

Figure 7.3: Elastic Response Spectrum at Building A for Blast sequence (ξ= 5 % critical),
(*Exp-Filt: Experimental response filtered between 3.05 to 6.11 Hz)

Table 7.5: Spectral acceleration at T1 = 0.245 s from elastic response spectrum along E-W direction (Blast Sequence)

E-W		
Response	S_a [g]	% Difference with LS-DYNA
LS-Dyna	0.055	0.000
Experimental	0.023	58.852
Exp-Filt	0.018	67.705

Table 7.6: Spectral acceleration at T2 = 0.204 s from elastic response spectrum along N-S direction (Blast Sequence)

N-S		
Response	S_a [g]	% Difference with LS-DYNA
LS-Dyna	0.057	0.000
Experimental	0.024	57.258
Exp-Filt	0.019	67.536

7.4.2.2 Collapse Sequence

Like the blast sequence, the elastic response spectrums of the numerical response for the collapse sequence has been compared with the corresponding elastic response spectrums obtained from the experimental response. While Figure 7.4 shows this comparison in frequency domain along E-W and N-S direction, Table 7.7 and Table 7.8 presents the summary of this comparison with respect to the spectral peaks at natural periods along the E-W and N-S direction. The spectral acceleration at the roof from the numerical response matches very well with the filtered experimental response. Table 7.7 also shows a smaller difference in the spectral acceleration between the numerical response and the experimental response at the natural period along E-W direction.

Although, the shape of the elastic response spectrum for numerical response along N-S matches with the corresponding elastic response spectrum of the filtered experimental response, the spectral acceleration at the natural period along N-S differ by 56.2 percent. The higher percentage difference along the N-S direction indicate that the numerical response along the N-S direction was attributed to a greater value of damping than the damping associated with the experimental response.

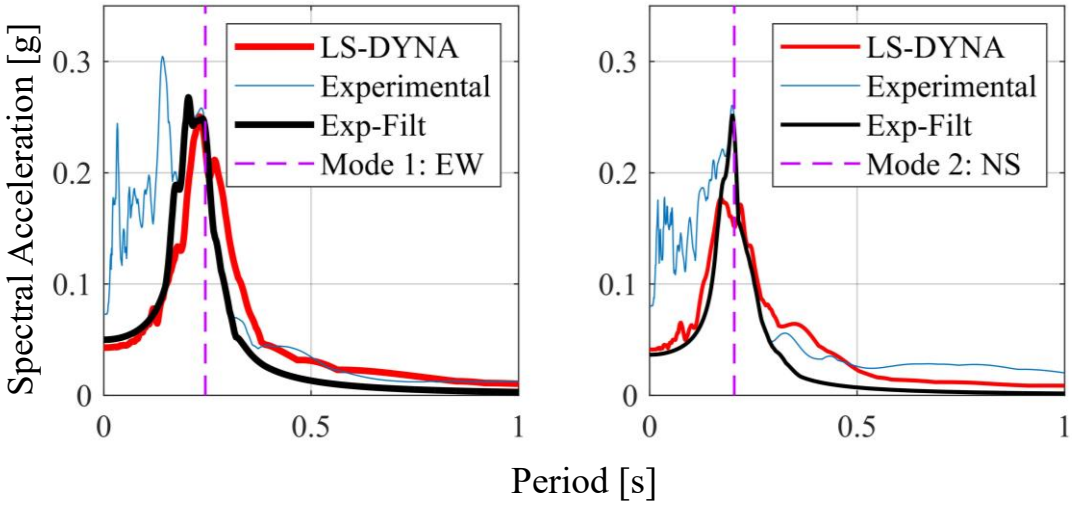

Figure 7.4: Elastic response spectrum at Building A for collapse sequence (ξ= 5 % critical), *(*Exp-Filt: Experimental response filtered between 3.05 to 6.11 Hz)*

Table 7.7: Spectral acceleration at T1 = 0.245 s from elastic response spectrum along E-W direction (Collapse Sequence)

E-W		
Response	S_a [g]	% Difference with LS-DYNA
LS-Dyna	0.222	0.000
Experimental	0.243	9.271
Exp. Filt	0.239	7.651

Table 7.8: Spectral acceleration at T2 = 0.204 s from elastic response spectrum along N-S direction (Collapse Sequence)

N-S		
Response	S_a [g]	% Difference with LS-DYNA
LS-Dyna	0.152	0.000
Experimental	0.248	62.788
Exp. Filt	0.238	56.213

7.5 Results: Building B

The roof acceleration response obtained from the numerical analysis of the 2DOF model of Building B has also been presented in both time domain and frequency domain like Section 7.4. The numerical response at the roof has been compared with the observed experimental response at the roof, and the comparison has been shown in both time and frequency domain.

7.5.1 Numerical Response vs. Experimental Response in Time Domain

The roof acceleration response for Building B along E-W and N-S direction obtained from the numerical analysis and the experimental observation have been compared in Figure 7.5. Table 7.9 and Table 7.10 shows the summary of peak acceleration values from Figure 7.5 in terms of the blast and collapse sequence along E-W and N-S.

The numerical and experimental acceleration responses to the blast sequence along the E-W direction reasonably agree with each other with only 4.9 % difference between the peak values. However, the experimental acceleration response along the N-S

direction is much smaller compared to the corresponding numerical response. This indicates that a higher value of damping could have been associated with the experimental response when compared with the numerical response. Further, the minimal value of experimental response along the N-S direction could also be due to the original structure not responding in a global translation mode such that the location of the sensor located on the third floor of Building B experienced a minimal response. In contrast to the original structure, the 2DOF tend to show a global translation mode along the N-S direction and hence a higher value of the acceleration response.

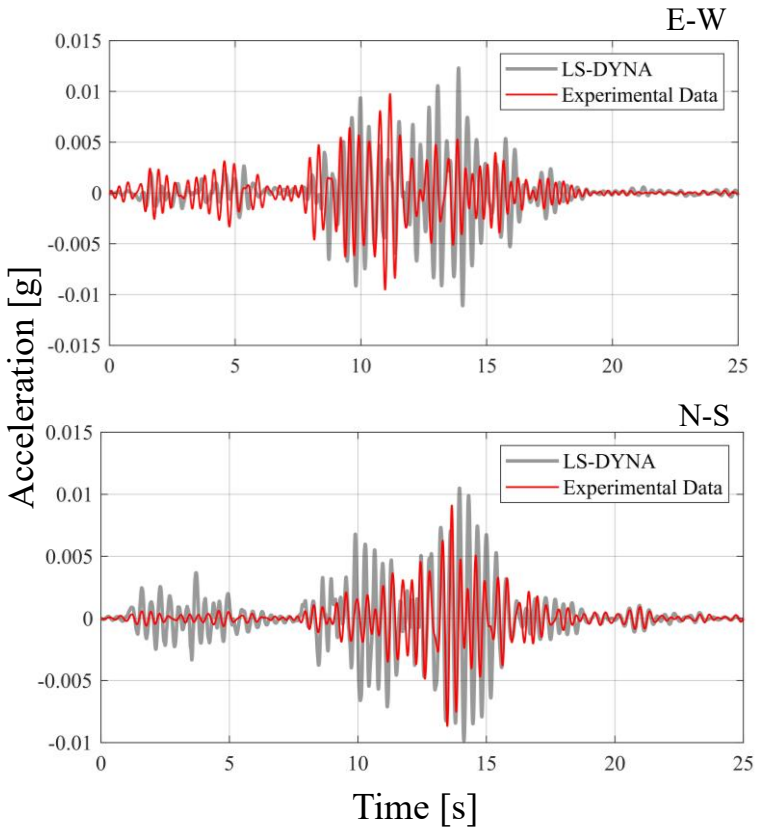

Figure 7.5: Comparison of acceleration time history for Building B: LS-DYNA vs. Exp-Filt
(*Exp-Filt: Experimental response filtered between 2.02 to 3.45 Hz)

Table 7.9: Peak acceleration values: LS-DYNA vs. Exp-Filt along E-W *(*Exp-Filt: Experimental response filtered between 2.02 to 3.45 Hz)*

E-W				
Response Data	Blast		Collapse	
	Peak Acc. [g]	% Diff	Peak Acc. [g]	% Diff
LS-Dyna	0.003	4.858	0.012	30.836
Experimental Data	0.003		0.009	

Table 7.10: Peak acceleration values: LS-DYNA vs. Exp-Filt along N-S *(*Exp-Filt: Experimental response filtered between 2.02 to 3.45 Hz)*

N-S				
Response Data	Blast		Collapse	
	Peak Acc. [g]	% Diff	Peak Acc. [g]	%Diff
LS-Dyna	0.004	84.071	0.010	18.255
Experimental	0.001		0.009	

7.5.2 Numerical Response vs. Experimental Response in Frequency Domain

A comparison of the numerical response with the observed experimental response at the roof level has been presented in terms of the blast and collapse sequence. The experimental response is presented in its original form, as previously discussed in Chapter 5, as well as bandpass filtered between 2.02 to 3.45 Hz to facilitate comparison with the 2DOF numerical model.

7.5.2.1 Blast Sequence

Figure 7.6 shows the comparison of the elastic response spectrum between the filtered experimental response and the numerical response during the blast sequence. As observed in the time domain of the blast sequence along the N-S direction, the elastic response spectrum for the numerical response also shows a much higher spectral acceleration than the filtered experimental response. However, the percentage difference of the spectral acceleration for the numerical and the filtered experimental response at the natural period along E-W is comparatively lower than the percentage difference of spectral accelerations at the natural period along N-S direction. Table 7.1 and Table 7.12 shows the summary of spectral acceleration values from Figure 7.6 at natural periods along E-W and N-S direction.

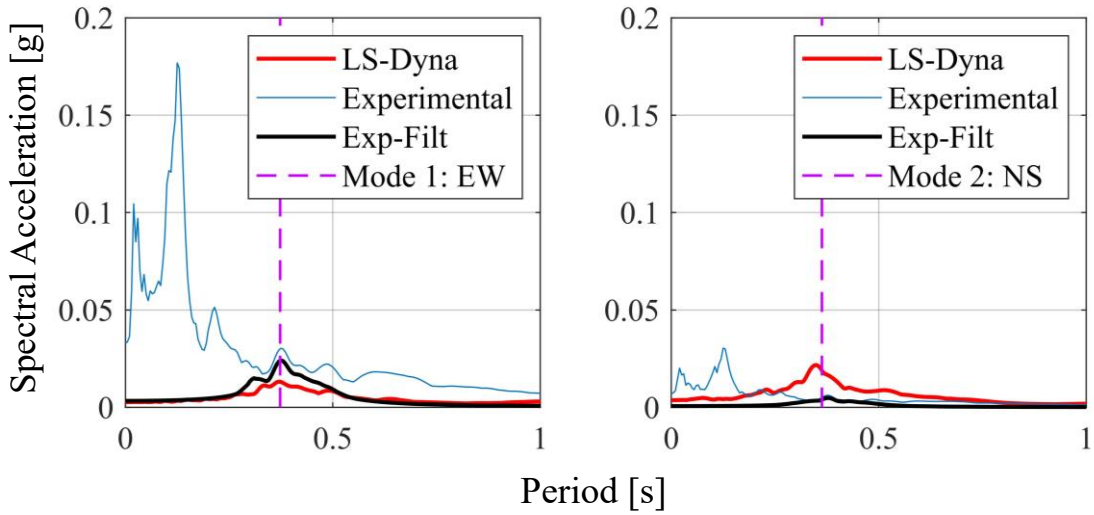

Figure 7.6: Elastic Response Spectrum at Building B for Blast sequence (ξ= 5 % critical),
(*Exp-Filt: Experimental response filtered between 2.02 to 3.45 Hz)

Table 7.11: Spectral acceleration at T1 = 0.373 s from elastic response spectrum along E-W direction (Blast Sequence)

E-W		
Response	Sa [g]	% Difference with LS-DYNA
LS-Dyna	0.018	0.000
Experimental	0.030	73.140
Exp-Filt	0.024	33.788

Table 7.12**: Spectral acceleration at T2 = 0.363 s from elastic response spectrum along E-W direction (Blast Sequence)**

N-S		
Response	Peak Sa [g]	% Difference with LS-DYNA
LS-Dyna	0.028	0.000
Exp-Filt	0.005	83.101
Exp. Filt	0.004	87.201

7.5.2.2 Collapse Sequence

Figure 7.7 shows the comparison of the numerical response and the experimental response of Building B in the frequency domain during the collapse sequence. The elastic response spectrum for the numerical response along the EW direction shows a better match when compared to the elastic response spectrum along the NS direction. Table 7.13 and Table 7.14 shows the summary of spectral acceleration values from Figure 7.7 at the natural periods along E-W and N-S direction. The percentage difference of the spectral acceleration value between the numerical response and the filtered experimental

response is comparatively less along the NS direction when compared to the EW direction.

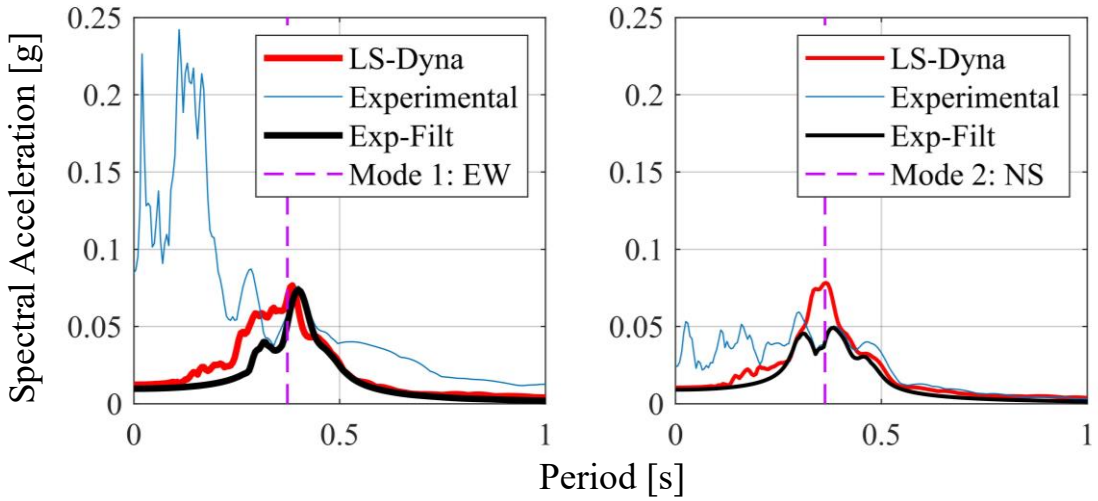

Figure 7.7: Elastic Response Spectrum at Building B for Collapse sequence (ξ= 5 % critical), *(*Exp-Filt: Experimental response filtered between 2.02 to 3.45 Hz)*

Table 7.13: Spectral acceleration at T1 = 0.373 s from elastic response spectrum along E-W direction (Collapse Sequence)

E-W		
Response	Sa [g]	% Difference with LS-DYNA
LS-Dyna	0.082	0.000
Experimental	0.058	29.475
Exp-Filt	0.052	36.559

Table 7.14: Spectral acceleration at T1 = 0.373 s from elastic response spectrum along E-W direction (Collapse Sequence)

N-S		
Response	Sa [g]	% Difference with LS-DYNA
LS-Dyna	0.112	0.000
Experimental	0.040	63.973
Exp-Filt	0.040	64.473

7.6 Conclusion

Key observations and conclusions made from the numerical analysis of Building A and Building B are summarized as follows:

1. The overall trend of the numerical response obtained for Building A and Building B indicate that the 2DOF models for both buildings tend to represent the experimental response better when subjected to collapse-induced ground motions. The numerical models for both buildings tend to show comparable response, especially along E-W direction, when subjected to the collapse-induced ground motion which has comparatively lower frequency compared to the blast-induced ground motion. The percentage difference of spectral acceleration between the numerical response and experimental response at natural period along E-W direction is below 30 % for Building A and Building B, when considering the collapse sequence. However, the percentage difference of spectral acceleration between the numerical response and experimental response at natural period along

E-W is above 60 % for Building A and Building B, when considering the blast sequence.

2. A lumped mass numerical modeling approach is more efficient in representing the lower modes of vibration of a structure that is dominated by the global vibration modes of the structure. The higher mode response of a structure is usually dominated by the local modes associated with the elemental vibration of a structure that cannot be represented by a 2DOF model. This is one key reason that a higher difference is observed between the experimental response and the numerical response when the numerical model is subjected to high-frequency blast-induced ground motions.
3. Although the numerical model seems to perform better for low-frequency excitations, a significant amplitude difference is evident in the spectral acceleration response between the numerical and the experimental response along the N-S direction. The amplitude difference could be attributed to the uncertainty associated with the assumption of damping in the numerical model.
4. The overall difference observed between the numerical response and the experimental response could be attributed to a wide array of factors. Some of these key factors are:
    - Degree of detail of the numerical modeling.
    - Type of damping assumed in the numerical model.
    - Absence of the soil domain in the numerical model that could be resulting in a frequency shift between the numerical response and the experimental response.

- Possible differences between the actual ground motion exciting the structure and the ground motions obtained from the free field positions.

CHAPTER 8 – CONCLUSIONS

8.1 Conclusions

The study of the response of the adjacent structures during the controlled implosion of Cather and Pound halls has provided critical insights over the understanding of the response of structures to the blast and progressive collapse of the multi-story structures. Primary conclusions drawn from the observed effects on the adjacent structures during the implosion and collapse of the full-scale 13-story reinforced structures are as follows:

- Collapse sequence of the demolition of the two 13-story structures dominated the observed response at all free field positions and the response observed within all the adjacent structures. Pulse-like behavior was evident in the observed response at the FF. Pos. 1 along vertical as well as N-S direction. This pulse-like behavior can be attributed to the progressive collapse of floors of two 13-story structures with uniform story heights. The fact that the progressive collapse was leaning predominantly on along the N-S direction, pulse-like behavior is observed in N-S direction in addition to the vertical direction at FF. Pos. 1.
- An exponential decay of the ground motions induced during the implosion was observed where FF. Pos. 3 at Building C recorded least response compared to all other free field positions.
- The ground motions induced due to the blast sequence showed relatively higher frequency content than the collapse induced ground motions. The high-frequency of the ground motions was distinctly observed in the frequency domain of the

response observed at FF. Pos. 1 and FF. Pos. 2. In general, the blast induced ground motions showed dominant frequencies with a lower bound of 10 Hz, and the collapse induced ground motions showed dominant frequencies as low as 2 Hz.

- The structural response at Building A and Building B show an attenuated response during the blast sequence along N-S direction when compared to the ground motions at their corresponding free field positions. The lower response to the blast sequence can be attributed to the short wavelengths of the high-frequency blast induced ground motions which are unable to uniformly excite the structure at its base in that direction.
- Contrary to the response along N-S direction, both Building A and Building B show an unexpected amplified response to the high-frequency blast-induced ground motions along the E-W direction. The amplified response in E-W direction indicates the interference of the airblast wave in the observed response of Building A and Building B during the blast sequence.
- The numerical modeling of the adjacent structures using a 2DOF lumped mass model indicates that the 2DOF model tend to predict experimental response better when subjected to low-frequency excitations.

8.2 Future Work

Recommendations for future work in this area include:

- The experimental dataset of the study can be used in the detail finite element analysis of the adjacent structures to understand the phenomenon of soil-structure interaction and structure-soil-structure-interaction.
- Detailed numerical modeling of the adjacent structures could investigate the higher mode response of the adjacent structures during the blast sequence.
- The experimental dataset in conjunction with finite element analysis can be used in a parametric study to understand the effect of individual parameters like system properties of the structure, properties of the soil domain, intensity of the implosion on the response of individual structures and a cluster of structures.
- The experimental dataset can be extended to understand response of structures to earthquake motions in an urban environment.

REFERENCES

Abdel-Ghaffar, A. M., and Scanlan, R. H. (1985). “Ambient Vibration Studies of Golden Gate Bridge: I. Suspended Structure.” *Journal of Engineering Mechanics*, 111(4), 463–482.

Abrahamson, N.A. (1985). “Estimation of Seismic Wave Coherency and Rapture Velocity using SMART-1 Strong Motion Array Recording.” *Report No. UCB/EERC-85-02*, Earthquake Engineering Research Center, University of California at Berkeley.

ARTeMIS Modal. (2019). Structural Vibration Solutions A/S, Denmark.

Beskos, D. (1993). "Applications of the Boundary Element Method in Dynamic Soil-Structure Interaction." *Developments in Dynamic Soil-Structure Interaction*, 61-90.

Bendat, J. S., and Piersol, A. G. (1993). *Engineering Applications of Correlation and Spectral Analysis*. J. Wiley, New York.

Bhattacharya, K., Dutta, S., and Dasgupta, S. (2004). "Effect of soil-flexibility on dynamic behaviour of building frames on raft foundation." *Journal of Sound and Vibration*, 274(1-2), 111-135.

Bolisetti, C. (2010). "Numerical and Physical Simulations of Soil-Structure Interaction." M.S. Thesis, University at Buffalo, The State University of New York, Buffalo, New York.

Bolisetti, C., and Whittaker, A. S. (2015). "Site Response, Soil-Structure Interaction and Structure-Soil-Structure Interaction for Performance Assessment of Buildings and Nuclear Structures." *MCEER-15-0002*, University at Buffalo, Buffalo, NY.

Bommer, J., and Martínez-Pereira, A. (1999). "The Effective Duration of Earthquake Strong Motion." *Journal of Earthquake Engineering*, 3(2), 127-172.

Brincker, R., Zhang, L., and Anders, P. (2000). "Modal Identification from Ambient Responses using Frequency Domain Decomposition." *Proc., International Modal Analysis Conference (IMAC XVIII)*, San Antonio, Texas, 625-626.

Brownjohn, J. M. W., Dumanoglu, A. A., and Severn, R. T. (1992). "Ambient Vibration Survey of the Fatih Sultan Mehmet (Second Bosporus) Suspension Bridge." *Earthquake Engineering & Structural Dynamics*, 21(10), 907–924.

Brownjohn, J. M. W. (2002). "Ambient Vibration Studies for System Identification of Tall Buildings." *Earthquake Engineering & Structural Dynamics*, 32(1), 71–95.

Çelebi, M. (1993a). "Seismic Responses of Two Adjacent Buildings. I: Data and Analyses." *Journal of Structural Engineering*, 119(8), 2461-2476.

Çelebi, M. (1993b). "Seismic Responses of Two Adjacent Buildings. II: Interaction." *Journal of Structural Engineering*, 119(8), 2477-2492.

Chang, C., Chang, T., and Zhang, Q. (2001). "Ambient Vibration of Long-Span Cable-Stayed Bridge." *Journal of Bridge Engineering*, 6(1), 46-53.

Chaudhary, M., Abe, M., Fujino, Y., and Yoshida, J. (2000). "System Identification of Two Base-Isolated Bridges using Seismic Records." *Journal of Structural Engineering*, 126(10), 1187-1195.

Chen, Z., Hutchinson, T. C., Trombetta, N. W., Mason, H. B., Bray, J. D., Jones, K. C., Bolisetti, C., Whittaker, A. S., Choy, B. Y., Kutter, B. L., Feigel, G. L.,

Montgomery, J., Patel, R. J., and Reitherman, R. D. (2010). "Seismic Performance Assessment in Dense Urban Areas: Evaluation of Nonlinear Building-Foundation Systems using Centrifuge Tests." *Proc., Fifth International Conference on Recent Advances in Geotechnical Earthquake Engineering and Soil Dynamics*, San Diego, California.

Clouteau, D., Aubry, D. (1992). “A Subdomain Approach to Dynamic Soil–Structure Interaction.” *Recent advances in earthquake engineering and structural dynamics*, Ouest Editions/AFPS, Nantes, 251-272.

Clouteau, D., Aubry, D. (2003). “Computational Soil–Structure Interaction.” *Boundary Element Methods for Soil-Structure Interaction*, Kluwer Academic Publishers, Dordrecht, 61-126.

de Barros, F., and Enrique Luco, J. (1995). "Identification of Foundation Impedance Functions and Soil Properties from Vibration Tests of the Hualien Containment Model." *Soil Dynamics and Earthquake Engineering*, 14(4), 229-248.

Dowding, C., Aimone-Martin, C., Meins, B., and Hamdi, E. (2018). "Large Structure Response to High Frequency Excitation from Rock Blasting." *International Journal of Rock Mechanics and Mining Sciences*, 111, 54-63.

Dutta, S., Bhattacharya, K., and Roy, R. (2004). "Response of low-rise buildings under seismic ground excitation incorporating soil–structure interaction." *Soil Dynamics and Earthquake Engineering*, 24(12), 893-914.

Elseman I. A. (2000). “Measurement and Analysis of the Effect of Ground Vibrations Induced by Blasting at the Limestone Quarries of the Egyptian Cement Company.” *Proc., ICEHM2000,* Cairo University, Egypt.

Faramarzi, F., Ebrahimi Farsangi, M., and Mansouri, H. (2014). "Simultaneous Investigation of Blast Induced Ground Vibration and Airblast Effects on Safety Level of Structures and Human in Surface Blasting." *International Journal of Mining Science and Technology*, 24(5), 663-669.

Ganuza, E. A. B. (2006). "Seismic Behavior of Hybrid Lateral-Force-Resisting Systems." M.S. Dissertation, University at Buffalo, The State University of New York, Buffalo, New York.

Gazetas, G. (1991). "Foundation Vibrations." *Foundation Engineering Handbook,* Ed. H. Fang, Kluwer Academic Publishers, Norwell, Massachusetts.

Hao, H., Wu, Y., Ma, G., and Zhou, Y. (2001). "Characteristics of Surface Ground Motions Induced by Blasts in Jointed Rock Mass." *Soil Dynamics and Earthquake Engineering*, 21(2), 85-98.

Jacobsen, N., Andersen, P., and Brincker, R. (2007). "Using Enhanced Frequency Domain Decomposition as a Robust Technique to Harmonic Excitation in Operational Modal Analysis." *Proc., International Operational Modal Analysis Conference (IOMAC),* Copenhagen, Denmark.

Jaishi, B., Ren, W.-X., Zong, Z.-H., and Maskey, P. N. (2003). “Dynamic and Seismic Performance of Old Multi-Tiered Temples in Nepal.” *Engineering Structures*, 25(14), 1827–1839.

Jennings, P. C., and Bielak, J. (1973). "Dynamics of Building-Soil Interaction." *Bulletin of the Seismological Society of America*, 63(1), 9-48.

Karabalis, D., and Mohammadi, M. (1998). "3-D Dynamic Foundation-Soil-Foundation Interaction on Layered Soil." *Soil Dynamics and Earthquake Engineering*, 17(3), 139-152.

Kobori T., Minai R., Kusakabe K. (1977). "Dynamical Cross-Interaction Between Two Foundations." *Proc., Sixth world conference on earthquake engineering*, New Delhi, India, 1484–1489.

Kramer, S. L., and Stewart, J. P. (2004). "Geotechnical Aspects of Seismic Hazards." *Earthquake Engineering from Engineering Seismology to Performance-Based Engineering*, eds. Y. Bozorgnia, and V. V. Bertero, CRC Press.

Lehmann, L., and Antes, H. (2001). "Dynamic Structure-Soil-Structure Interaction Applying the Symmetric Galerkin Boundary Element Method (SGBEM)." *Mechanics Research Communications*, 28(3), 297-304.

Livermore Software Technology Corporation (LSTC). (2019). "LS-DYNA Theory Manual." Livermore Software Technology Corporation, Livermore, California.

Lin, H., -T., Roesset, J. M., and Tassoulas, J. L. (1987). "Dynamic Interaction Between Adjacent Foundations." *Earthquake Engineering and Structural Dynamics*, 15, 323-343.

Luco, J. E., and Contesse, L. (1973). "Dynamic Structure-Soil-Structure Interaction." *Bulletin of the Seismological Society of America*, 63(4), 1289-1303.

Lysmer, J., Ostadan, F., and Chin, C. (1999). Computer Program SASSI2000 - A System for Analysis of Soil-Structure Interaction, University of California, Berkeley, California.

Matthees, W., and Magiera, G. (1982). "A Sensitivity Study of Seismic Structure-Soil-Structure Interaction Problems for Nuclear Power Plants." *Nuclear Engineering and Design*, 73, 343-363.

Mizuno H. (1980). “Effects of Structure–Soil–Structure Interaction during Various Excitations.” *Proc., of the seventh world conference on earthquake engineering*, Istanbul, Turkey, 149–156.

Mylonakis, G., and Gazetas, G. (2000). "Seismic Soil-Structure Interaction: Beneficial or Detrimental?." *Journal of Earthquake Engineering*, 4(3), 277-301.

Nateghi, R. (2011). "Prediction of Ground Vibration Level Induced by Blasting at Different Rock Units." *International Journal of Rock Mechanics and Mining Sciences*, 48(6), 899-908.

Padron, L. A., Aznarez, J. J., and Maeso, O. (2009). "Dynamic Structure Soil-Structure Interaction between Nearby Piled Buildings under Seismic Excitation by BEM-FEM Model." *Soil Dynamics and Earthquake Engineering*, 29, 1084-1096.

Peeters, B., and De Roeck, G. (2001). "Stochastic System Identification for Operational Modal Analysis: A Review." *Journal of Dynamic Systems, Measurement, and Control*, 123(4), 659.

Pitilakis K., Kirtas E., Sextos A., Bolton M., Madabhushi G., Brennan A. (2004) "Validation by Centrifuge Testing of Numerical Simulations for Soil–Foundation–Structure Systems." *Proc., 13th world conference on earthquake engineering*, Vancouver, Canada.

Pitilakis, D., Dietz, M., Wood, D., Clouteau, D., and Modaressi, A. (2008). "Numerical Simulation of Dynamic Soil–Structure Interaction in Shaking Table Testing." *Soil Dynamics and Earthquake Engineering*, 28(6), 453-467.

Ren, W., Harik, I., Blandford, G., Lenett, M., and Baseheart, T. (2004). "Roebling Suspension Bridge. II: Ambient Testing and Live-Load Response." *Journal of Bridge Engineering*, 9(2), 119-126.

Ren, W., Zhao, T., and Harik, I. (2004). "Experimental and Analytical Modal Analysis of Steel Arch Bridge." *Journal of Structural Engineering*, 130(7), 1022-1031.

Siskind D.E., Stagg M.S., Koop J.W., Dowding C.H. (1980). "Structure Response and Damageproduced by Ground Vibration from Surface Mine Blasting." *Report of Investigations 8485*, US Bureau of Mines, Washington DC.

Siskind D.E., Stachura V.J., Stagg M.S., Koop J.W., Dowding C.H. (1980). "Structure Response and Damage Produced by Ground Vibration from Surface Mine Blasting." *Report of Investigations 8507*, US Bureau of Mines, Washington DC.

Trifunac, M. D., Stewart, J. P., Fenves, G. L., and Seed, R. B. (2000). "Seismic Soil-Structure Interaction in Buildings. I: Analytical Methods; Seismic Soil-Structure Interaction in Buildings. II: Empirical Findings." *Journal of Geotechnical and Geoenvironmental Engineering*, 126(7), 668–672.

USGS. (2019). http://usgs.maps.arcgis.com/apps/webappviewer/index.html?id=8ac19bc334f747e486550f32837578e1 (Apr. 8, 2019).

Wang, S., and Schmid, G. (1992). "Dynamic Structure-Soil-Structure Interaction by FEM and BEM." Computational Mechanics, 9(5), 347-357.

Wong, H. L., and Trifunac, M. D. (1975). "Two-Dimensional, Antiplane, Building-Soil-Building Interaction for Two or More Buildings and for Incident Plane SH Waves." *Bulletin of the Seismological Society of America*, 65(6), 1863-1885.

APPENDIX A

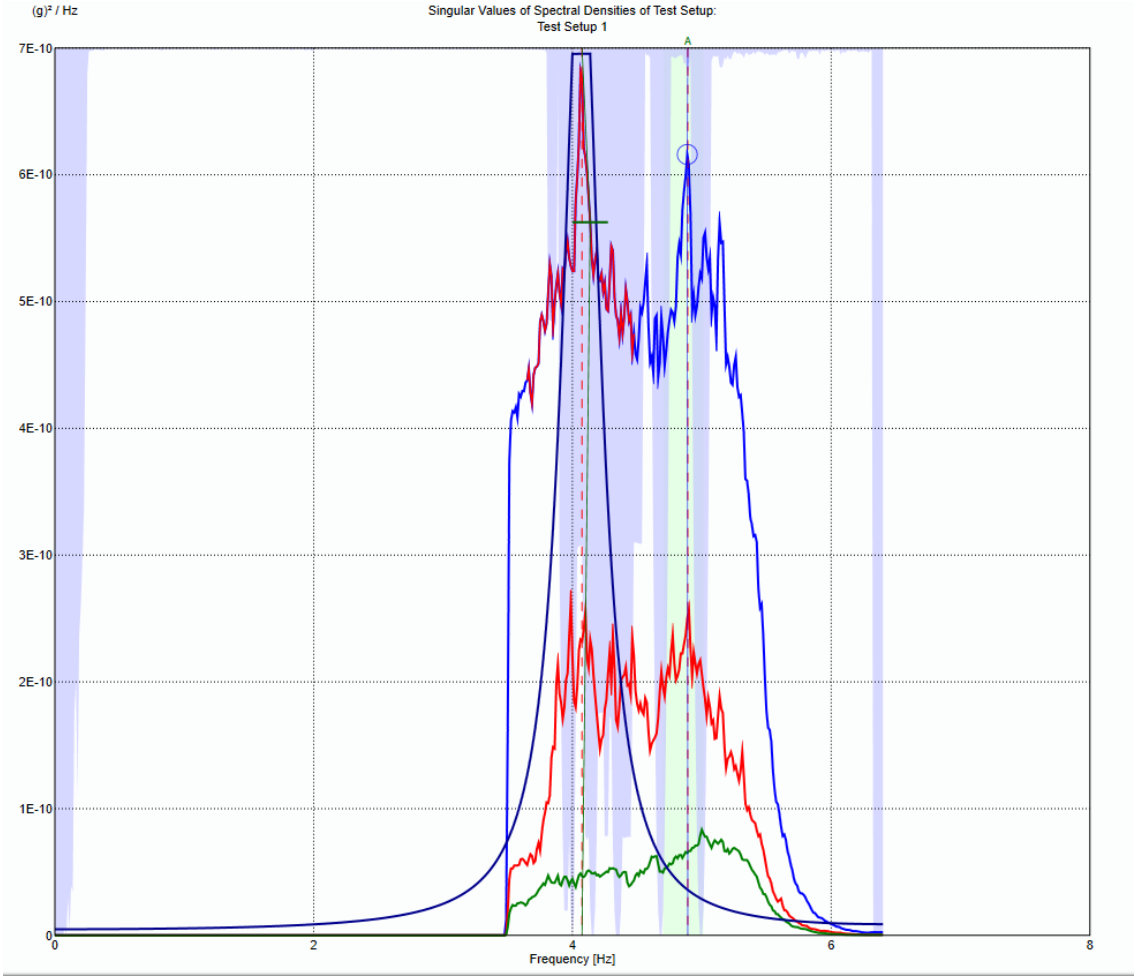

Figure A.1. Curve fitted auto spectral density function for Mode 1 (4.074 Hz) - Building A

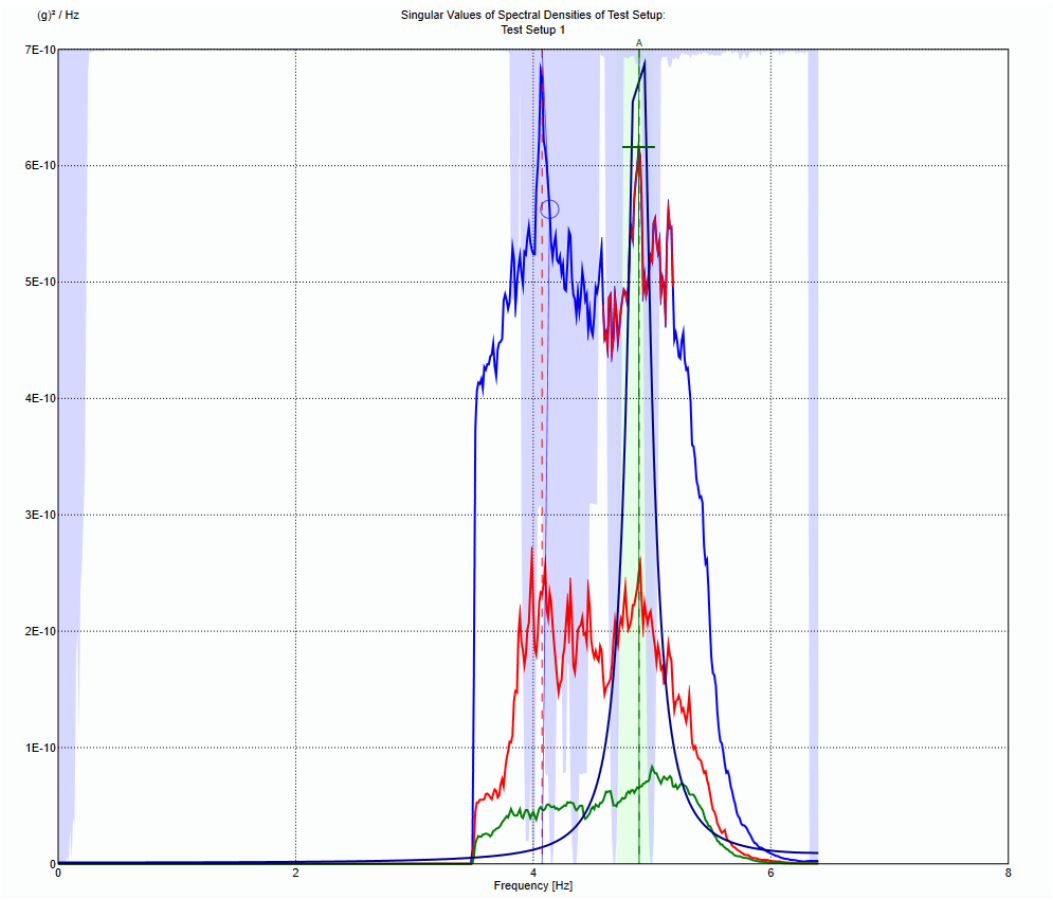

Figure A.2. Curve fitted auto spectral density function for Mode 1 (4.892 Hz) - Building A